Geotechnical aspects of reconnaissance findings after 2020 January 24th, M6.8 Sivrice–Elazig–Turkey earthquake

Kemal Onder Cetin[1] · Elife Cakir[1] · Makbule Ilgac[1] · Gizem Can[1] ·
Berkan Soylemez[1] · Alaa Elsaid[1] · Faik Cuceoglu[1,2] · Zeynep Gulerce[1] ·
Aysegul Askan[1] · Seckin Aydin[2] · Mesut Gor[3]

Abstract

On January 24, 2020, Sivrice–Elazig–Turkey earthquake occurred along the East Anatolian Fault Zone. The moment magnitude of the event was reported as 6.8. This paper documents reconnaissance findings performed immediately after the event. Investigated sites namely, Lake Hazar shores, Karakaya Dam Reservoir–Euphrates River shores, Malatya–Battalgazi district and its villages, and Elazig Downtown are predicted to be shaken by rock peak ground acceleration, $PGA_{VS30=1100\ m/s}$, levels of 0.12–0.42 g, 0.05–0.11 g, 0.05 g, and 0.08 g respectively. The documented geotechnical field performances vary from widespread liquefaction-induced sand boils and lateral spreading, to no signs of surface manifestations of permanent ground deformations or soil liquefaction. In Battalgazi district and Elazig Downtown, the foundation performances vary from no signs of permanent ground deformations to 1–3 cm settlements, and 1–2 cm lateral movements. Additionally, the hydraulic structures inspected are estimated to be shaken by $PGA_{VS30=1100\ m/s}$ levels of 0.03–0.23 g. Other than a minor longitudinal cracking along a limited section along the crest of a homogeneous earthfill dam, no apparent signs of permanent ground deformations were reported. Last but not least, a number of rock falls were mapped, based on back analyses of which probable peak ground velocities at these rockfall sites were speculated.

Keywords Reconnaissance · Sivrice earthquake · Liquefaction · Hydraulic structures · Foundations · Seismic performance

List of symbols

a_{max}	Maximum ground acceleration
C_B	Correction factor for borehole diameter
C_c	Compression index

✉ Kemal Onder Cetin
  ocetin@metu.edu.tr

1   Middle East Technical University, Universiteler Mah. Dumlupınar Bulv., 06800 Cankaya, Ankara, Turkey

2   The General Directorate of Hydraulic State Works (DSI), Devlet Mah., Inonu Bulv., Ankara, Turkey

3   Firat University, 23119 Elazig, Turkey

C_C	Coefficient of curvature
C_E	Correction factor for hammer energy ratio
C_r	Recompression index
C_R	Correction factor for rod lenght
C_N	Correction factor for overburden pressure
C_S	Correction factor for sampling method
C_U	Coefficient of uniformity
$CRR_{\sigma'_v=1\ atm,\ M=7.5,\ PL=50\%}$	Cyclic resistance ratio adjusted to $\sigma'_v = 1$ atm, $M = 7.5$, $PL = 50\%$
$CSR_{\sigma'v,M}$	Cyclic stress ratio at a given vertical effective stres and moment magnitude
$CSR_{\sigma'v=1\ atm,\ M=7.5}$	Cyclic stress ratio normalized to 1 atm vertical effective stress for a M7.5 event
$d_{crt.}$	Critical depth
D_{10}	Paticle size corresponding to 10% finer on the cumulative particle size distribution curve
D_{30}	Paticle size corresponding to 30% finer on the cumulative particle size distribution curve
D_{60}	Paticle size corresponding to 60% finer on the cumulative particle size distribution curve
FC	Fines content
FS	Factor of safety
K_M	Magnitude scaling factors
K_σ	Overburden correction factor
M	Moment magnitude of the earthquake
N	Measured standard penetration test blow counts
$N_{1,60}$	Normalized (overburden, equipment and procedure corrected) standard penetration test blow counts
$N_{1,60,CS}$	Equivalent clean sand normalized standard penetration test blow counts
P_L	Probability of liquefaction triggering
PGA_{475}	PGA for 475-year return period
PGA_{72}	PGA for 72-year return period
$PGA_{VS30=1100\ m/s}$	Median PGA for $V_{S30} = 1100$ m/s
r_d	Stress reduction factor (aka: non-linear shear mass participation)
S_1	Coefficient factor for spectral acceleration at 1 s period
S_{D1}	Coefficient factor for design spectral acceleration at 1 s period
S_{DS}	Coefficient factor for design spectral acceleration at short period
S_S	Coefficient factor for spectral acceleration at short period
V_{S12}	Shear wave velocity of the upper 12 m
V_{S30}	Shear wave velocity of the upper 30 m
σ_v	Vertical total stress
σ_v'	Vertical effective stress
σ_p'	Preconsolidation pressure

1 Introduction and seismological setting

On January 24, 2020 at 17:55 (UTC) (20:55 local time), a moment magnitude (M) of 6.8 (according to AFAD, Disaster and Emergency Management Presidency; https://deprem. afad.gov.tr/depremdokumanlari/1831) or 6.7 (according to USGS; https://earthquake.usgs. gov/earthquakes/eventpage/us60007ewc/executive) earthquake occurred along the East Anatolian Fault Zone (EAFZ) of Turkey. EAFZ is a NE–SW striking, left-lateral intra-continental strike slip fault system, which extends between Karliova junction and Antakya at the NE corner of Mediterranean Sea (Saroglu et al. 1992). This system had been seis-mically quiet in the twentieth century. The 2020 Elazig–Sivrice earthquake is the largest magnitude event recorded on EAFZ in the last two centuries; therefore, the seismotectonic data complied after this earthquake may provide valuable input in fault segmentation and rupture forecast models (Pousse-Beltran et al. 2020). The mainshock of Elazig–Sivrice earthquake was followed by 206 aftershocks with M > 3 within 30 days after the event, as shown in Fig. 1. The aftershocks are distributed along a 70–80 km-long fault plane over EAFZ, specifically between Sivrice and Puturge towns. As revealed by MTA (2020), the surface deformations were observed for approximately 48 km along EAFZ, starting from Lake Hazar down to Puturge. Figure 1 indicates that the extent of these surface deforma-tions is consistent with the spatial distribution of aftershocks.

Duman and Emre (2013) defined two segments for EAFZ separated by releasing bend of Lake Hazar: Palu segment lying in between Palu and Lake Hazar (blue line in Fig. 1) and the Puturge segment located between Lake Hazar and Sincik (green line in Fig. 1) (Gul-erce et al. 2017). The epicenter of the mainshock is located on the Puturge segment, which was subjected to elevated stress levels due to 2010 Elazig–Kovancilar earthquake (M = 6.1)
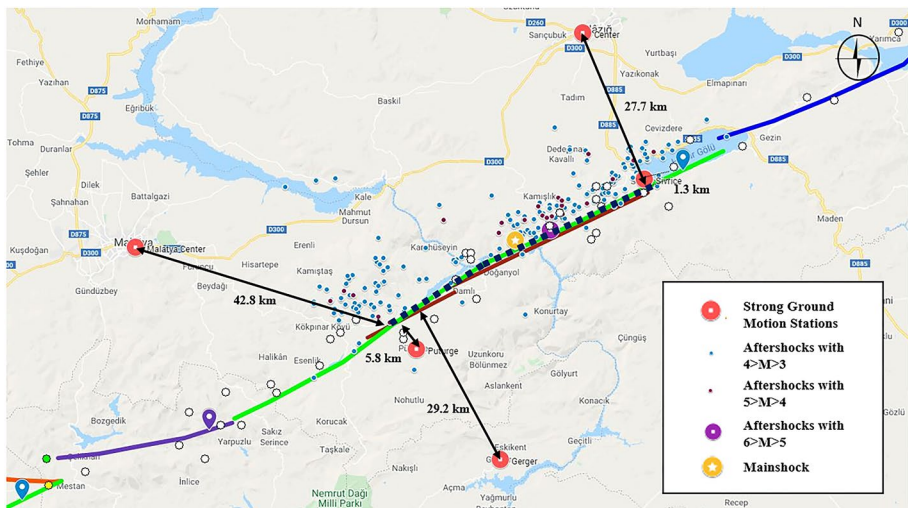
Fig. 1 Rupture plane of 2020 Elazig–Sivrice earthquake assessed by Pousse-Beltran et al. (2020) (solid red line), approximate location of the observed surface deformations at the field (dark blue dashed line) and the aftershocks with M > 3 occurred on the first 30 days after the mainshock, color-coded according to mag-nitude. Locations of the five strong motion stations with PGA > 0.05 g are shown with red pins. Blue and green lines are Palu and Puturge segments which are slightly modified for their termination points by Gul-erce et al. (2017). R_{JB} values for stations given in Table 1 are shown with black arrows

occurred on the Palu segment (Akkar et al. 2011). Pousse-Beltran et al. (2020) divided Puturge segment into two sub-segments with a small left step-over between Doganyol and Puturge, based on the analysis of Interferometric Synthetic Aperture Radar (InSAR) and optical satellite imagery, tele-seismic back-projections, regional moment tensors, and calibrated hypocentral relocations. It was argued that the 2020 Elazig–Sivrice earthquake was "not characteristic": larger ruptures on Puturge segment are possible, which should be taken into account in future seismic hazard assessment studies. Segmentation model and characteristic magnitude estimations of Gulerce et al. (2017) were consistent with this argument: the characteristic magnitude of the Puturge segment was estimated to vary between $M = 7.19$–7.23 due to different magnitude scaling relations and implemented in probabilistic seismic hazard assessment (PSHA).

The mainshock is recorded by 243 strong motion stations operated by AFAD; however, only seven stations have recorded peak ground accelerations (PGA) with engineering significance (PGA > 0.05 g), and only five stations are located within 50 km of the rupture plane (https://tadas.afad.gov.tr/, last accessed on October 7, 2020). Table 1 presents the horizontal component PGA values recorded at these five stations. The shear wave velocity profiles for selected stations were measured. The time-averaged shear wave velocity at the first 30 m (V_{S30}) for Puturge (ID#4404), Elazig Center (ID#2301), and Malatya Center (ID#4401) stations were documented by Sandikkaya et al. (2010). Similarly, the V_{S30} values of Sivrice (ID#2308) and Gerger (ID# 0204) stations were measured by Kurtulus et al. (2019). The rupture (R_{RUP}) and Joyner–Boore (R_{JB}) distances provided in Table 1 are calculated by using the rupture plane dimensions shown in Fig. 1 with the assumption that depth to the top of the rupture is equal to 0.5 km. It should be noted that the R_{JB} values estimated by Cheloni and Akinci (2020) are significantly different for Sivrice and Elazig Center stations, due to the uncertainty in the extent of the rupture plane through Lake Hazar. The 5%-damped elastic horizontal response spectra recorded at the selected stations are presented in Fig. 2.

The Turkish Seismic Hazard Map (TSHM) was updated in 2018 (Akkar et al. 2018), and it is being enforced as part of updated Turkish Building Earthquake Code (TBDY 2019) for assessing design-basis spectra of regular buildings since the beginning of 2019. The short period (S_S) and 1 s (S_1) ground motions in TSHM with 20% and 10% chance of exceedance in 50 years (corresponding to 72- and 475-year return periods, respectively) at the station locations are presented in Table 1 (https://tdth.afad.gov.tr, last accessed in February 11, 2020). To calculate the S_{DS} and S_{D1} values, the site amplification coefficients given in TBDY (2019) are taken into account, and the PGA values for both hazard levels are estimated as 40% of the corresponding S_{DS} values. Figure 2 shows that the recorded PGA values at Elazig Center, Puturge and Sivrice stations are approximately equal to the 72-year PGA values given in TSHM; while, the short period spectral accelerations are smaller than 72-year design spectra for all stations. Spectral accelerations at mid-long periods (T > 0.5 s) in Elazig Center and Gerger stations are very close to the 72-year design spectrum; however, the recorded mid-long period ground motions exceed the 72-year spectrum and reach up to the 475-year design spectrum in Puturge and Sivrice stations.

A recent study by Kale (2019) has utilized several ranking methods for comparing the predictive performance of ground motion models (GMMs) for shallow crustal and active tectonic regions with the Turkish strong motion database. Analysis results indicated that the regional Kale et al. (2015) model, the Turkey (TR)-adjusted version of the Boore and Atkinson (2008) model (Gulerce et al. 2016), and the global Chiou and Youngs (2014) model have better predictive performances when compared to other alternatives. To compare the distance attenuation of the recorded strong motions with the distance scaling of

**Table 1** A summary of strong ground motion stations' and recorded motions' characteristics

Stations				PGA (g)					V_{s30} (m/s)	72-year					475-year				
Station code	Name	Latitude	Longitude	N–S	E–W	R_{rup} (km)	R_{jb} (km)			S_S	S_1	S_{DS}	S_{D1}	PGA_{72}	S_S	S_1	S_{DS}	S_{D1}	PGA_{475}
2308	Sivrice	38.451	39.310	0.243	0.298	1.39	1.30	450		0.539	0.126	0.692	0.189	0.277	1.504	0.396	1.805	0.594	0.722
4404	Puturge	38.196	38.874	0.211	0.244	5.82	5.80	1380		0.548	0.122	0.493	0.098	0.197	1.578	0.403	1.42	0.322	0.568
0204	Gerger	38.029	39.035	0.096	0.112	29.2	29.2	555		0.344	0.085	0.447	0.127	0.179	0.883	0.233	1.06	0.35	0.424
2301	Elazig Center	38.670	39.193	0.121	0.143	27.7	27.7	407		0.342	0.097	0.445	0.146	0.178	0.912	0.257	1.094	0.386	0.438
4401	Malatya Center	38.349	38.335	0.074	0.088	42.8	42.8	481		0.316	0.086	0.411	0.129	0.137	0.836	0.23	1.087	0.345	0.35
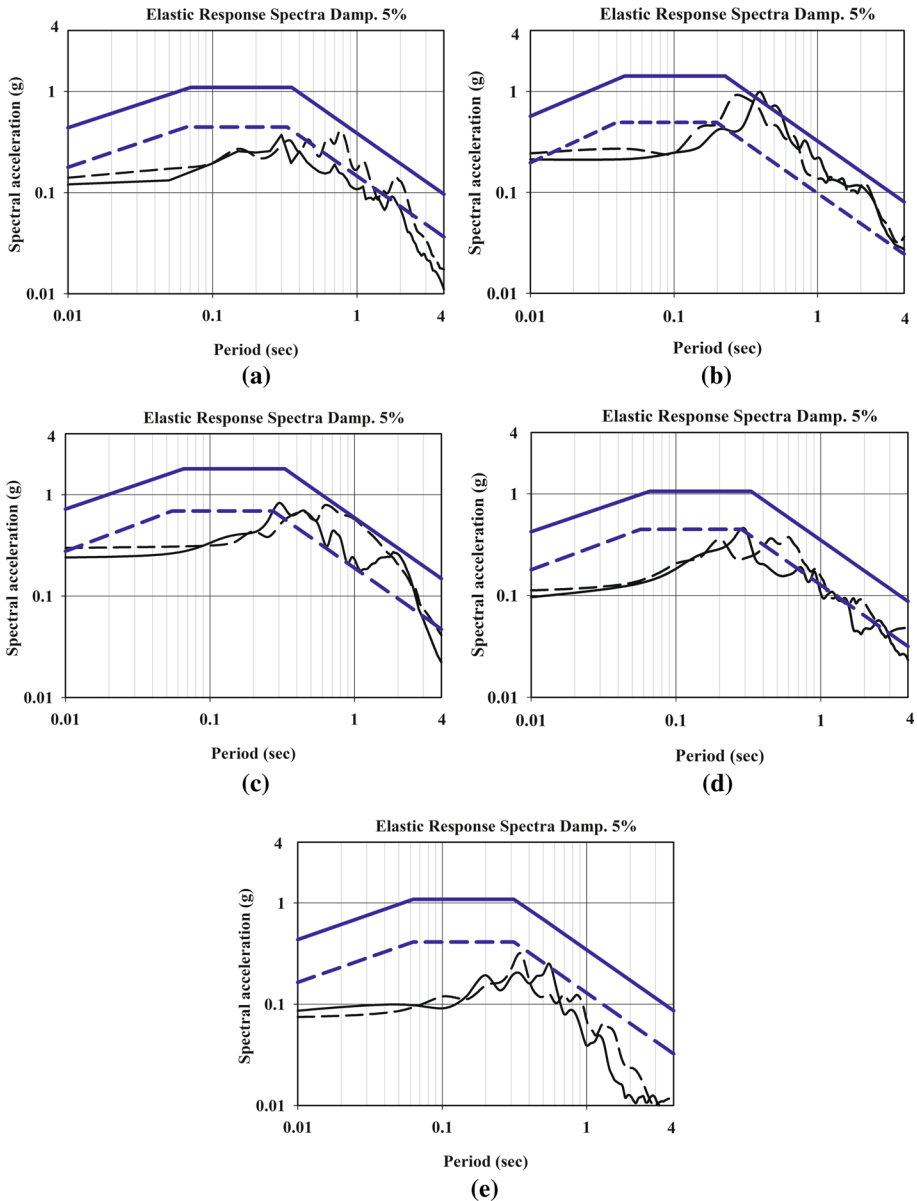
Fig. 2 Recorded 5% damped elastic response spectra and the 72-years and 475-years design spectra according to TBDY (2019) for **a** Elazig Center station (ID#2301), **b** Puturge station (ID#4404), **c** Sivrice station (ID#2308), **d** Gerger station (ID#0204), **e** Malatya Center station (ID#4401)

abovementioned GMMs, the recorded values are normalized to $V_{S30}=400$ m/s by using the site amplification scaling utilized in each GMM. Normalized PGA values from selected stations are compared with the median $\pm 1\sigma$ predictions of TR-adjusted Boore and Atkinson (2008), TR-adjusted Chiou and Youngs (2008), Boore et al. (2014), Chiou and Youngs

(2014) and Kale et al. (2015) models in Fig. 3a. According to Fig. 3a, the PGAs recorded in Puturge, Gerger and Elazig Center stations are equal to or very close to the median estimations of the tested GMMs. The PGA value recorded at the closest location to the epicenter, the Sivrice station, is closer to the lower bound of the range (median − 1σ) for all GMMs. This observation is consistent with the results of ground motion simulations for this event: simulated ground motion intensities for Sivrice station in Cheloni and Akinci (2020) are significantly higher than the recorded ones, especially at high frequencies. The PGA value recorded at Malatya Center station is also lower than the median estimations of
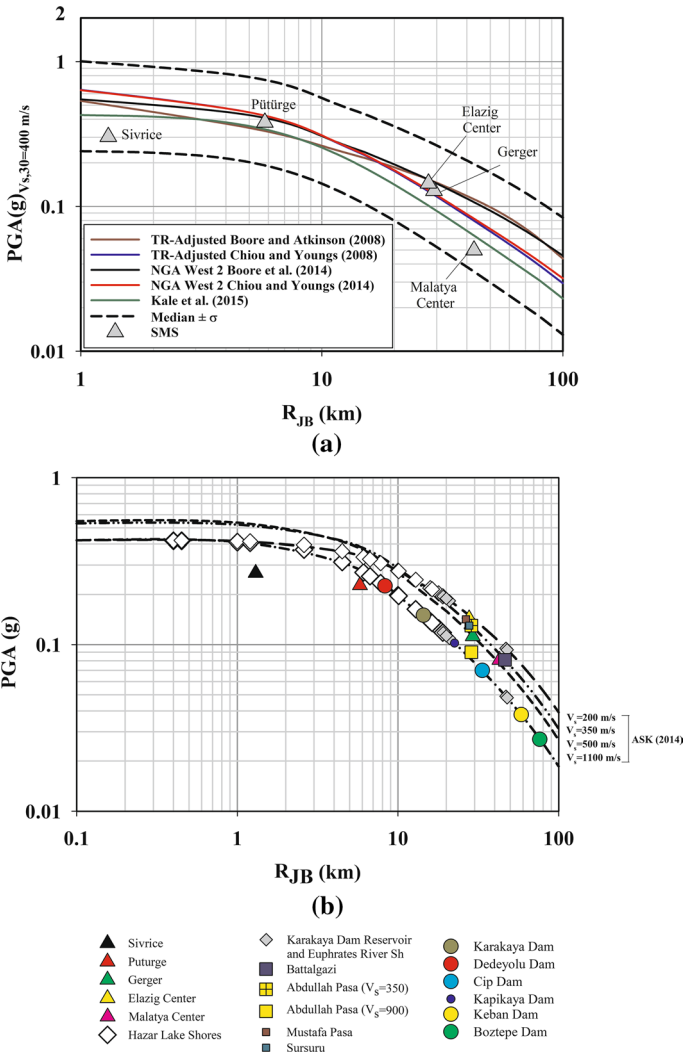
Fig. 3 **a** Median estimation of selected GMMs for $V_{S30} = 400$ m/s and recorded PGA values normalized to $V_{S30} = 400$ m/s at selected strong motion stations. Dashed lines show the lower and upper bound of median ± σ range for selected GMMs, **b** recorded and predicted PGA values at visited sites along with median estimations of ASK14 model for $V_{S30} = 200–1100$ m/s

GMMs. The distance attenuation plots given in Akkar et al. (2011) for 2010 Elazig–Kovan-cilar event and in Cheloni and Akinci (2020) for this earthquake indicated faster atten-uation beyond 50 km in the recorded ground motions. Figure 3b compares the recorded rotation independent average horizontal (GMRotD50) PGA values with the median predic-tions of Abrahamson et al. (2014) (ASK14) GMM for various V_{S30} values. The fit between recorded data and median predictions of the ASK14 model is satisfactory for $R_{RUP} > 10$ km and similar to the other GMMs; therefore, ASK14 model is used to estimate the intensity of ground shaking levels at visited soil, rock, earthfill and rockfill dam sites, which will be presented later in the manuscript.

After the event, Middle East Technical University (METU) Civil Engineering Depart-ment Geotechnical Reconnaissance team arrived the city of Elazig on the 31st of January to collect and document perishable data in the form of permanent ground deformations due to strong ground shaking, soil liquefaction or slope instability. Additionally, the seis-mic performances of earthfill and rockfill dams, tunnels and residential building foundation systems were documented. The reconnaissance route was mostly concentrated on soil sites, which are composed of young alluvial deposits. Hence, as shown in Fig. 4, Lake Hazar, Karakaya Reservoir and Euphrates River shores were visited and investigated. Although there are free field soil sites with high potential for liquefaction triggering in the vicinity of the shores of Lake Hazar and Euphrates River, due to lack of urbanization in these areas, the contribution of liquefaction triggering to observed structural damage is judged to be none, except for Sivrice Dock site, which will be presented next. The discussions of our findings will be presented separately under the performance of (a) potentially liquefiable
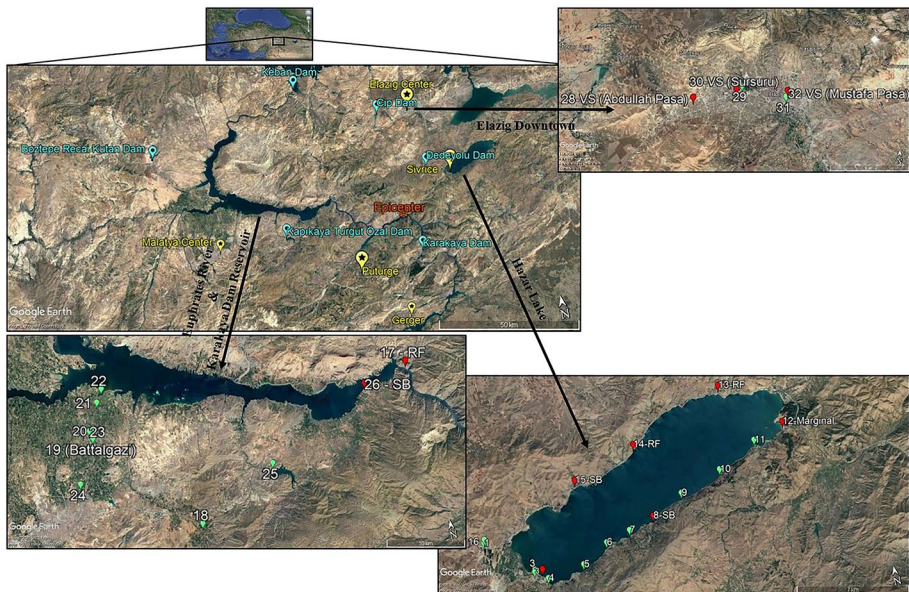
Fig. 4 A summary of ground failure observations along the shores of Lake Hazar, the shores of Karakaya Dam Reservoir and Euphrates River and Malatya–Elazig Route (Green pins indicate potentially liquefiable (alluvial), but non-liquefied sites, Red pins indicate sites with surface manifestation or soil liquefaction, *RF* rockfall, *LS* liquefaction-induced lateral spread, *VS* volumetric settlement, *SB* sand Boil), Google Earth, 2018

sites, (b) soil and rock slopes, (c) hydraulic structures, and (d) foundations in the next sections. These reconnaissance findings are hoped to contribute to the development of case history-based predictive models, which establish the basis of engineering assessments in seismic soil liquefaction triggering (e.g.: Seed et al. 1985; Cetin et al. 2018; Boulanger and Idriss 2012; Brandenberg et al. 2020), seismic performance assessments of soil slopes (e.g.: Saygili and Rathje 2008); and earth structures (Makdisi and Seed 1977).

2 Performance of potentially liquefiable soil sites

With the intent of identifying liquefied soil sites, the shores of Lake Hazar, Karakaya Dam Reservoir, and Euphrates River were visited. Seismically-induced soil liquefaction surface manifestations in the form of sand boils, excessive settlements and lateral spreading deformations were observed along the shores of the lake. At other potentially liquefiable alluvial sites, these surface manifestations were not evident. Table 2 presents a summary of these field performances. In this table, in addition to the coordinates of the sites, site specific PGA values were listed. In the estimation of site specific PGA values, event compatible ASK14 model is used along with the R_{jb} of the sites, as presented in Fig. 3b. Moreover, a summary of the field performances including: (1) triggering of liquefaction or not, (2) the magnitude of ground deformations, if any, (3) availability of site specific site investigation data in the form of borelogs is presented. Representative borelogs were identified considering the proximity of boreholes and site locations along with the similarities in the geological settings. Due to plastic nature of cohesive soil layers dominating the alluvial geological setting of Elazig and Malatya Downtown districts, only a limited number of potentially liquefiable sites and soil layers exist at these districts, and they did not liquefy during this event. The documentation of sites with surface manifestations of soil liquefaction and/or permanent ground deformations are presented in a more complete manner; whereas, for the ones lacking, no further discussion are given due to page limitations. However, readers are referred to Cetin et al. (2020) for accessing to a complete documentation and discussion of all these sites.

2.1 Surface manifestations of soil liquefaction

Seismically-induced lateral spreading and volumetric settlements were observed at partially inundated Sivrice Dock and its immediate neighboring beach. Observed ground failures were mapped as presented in Fig. 5, a more detailed discussion of which is presented in Cetin et al. (2020). The dock is underlain by gravelly fill, and due to lateral spreading and volumetric densification of the gravelly fill layer, both lateral and vertical displacements were observed and mapped, the magnitude of which varied in the range of 3–5.5 cm, and 2.5–7 cm. respectively.

Similarly, liquefaction-induced lateral spreading deformations, presented in Fig. 6, were mapped along a 90 m by 24 m shoreline neighboring to Sivrice Dock, with induced crack widths varying from 3 to 5 cm. The total maximum lateral deformation at the most critical section was mapped as 10–14 cm. Immediately in the south-east of this local beach, there is another beach, where no signs of permanent ground deformations or liquefaction manifestations were evident, as shown in Fig. 7. This beach was observed to have a milder slope when compared to the lateral spreading site.

Table 2 A summary of the potentially liquefiable sites and their seismic performances

Site Name (coordinates)	Median PGA (g) based on possible V_{S30}	Surface manifestation of liquefaction	Borelog available (proximity to the site)	Remark
Site 1 Sivrice Road (38°28'08.6"N 39°16'40.2"E)	0.31–0.36	No	No	Alluvial geological setting
Site 2 Sivrice Dock (38°26'53.2"N 39°18'53.4"E)	0.41–0.42	Yes, lateral spreading and volumetric settlement	Yes SK10 (0.11 km) SK4 (0.26 km) SK7 (0.28 km)	Both lateral (3–5.5 cm) and vertical (2.5–7 cm) displacements were mapped. Neighboring to Sivrice Dock, liquefaction-induced lateral spreading deformations were mapped along a 90 m by 24 m shoreline, with induced crack widths varying from 3 to 5 cm
Site 4 (38°26'32.0"N 39°19'11.4"E)	0.42	No	No	Surface geology is composed of volcanic rock
Site 6 (38°27'17.1"N 39°21'49.3"E)	0.31–0.36	No	No	Surface geology is composed of low plasticity clays
Site 7 (38°27'31.0"N 39°22'55.9"E)	0.27–0.34	No	No	
Site 8 (38°27'49.7"N 39°24'01.1"E)	0.23–0.31	Yes, sand boils	No	Sand boil samples were taken
Site 9 (38°28'22.2"N 39°25'24.9"E)	0.20–0.28	No	No	
Site 11 (38°29'37.1"N 39°29'02.3"E)	0.14–0.22	No	No	
Site 12 (38°29'58.5"N 39°30'24.6"E)	0.13–0.20	Yes, sand boils	No	Sand boil samples were taken
Site 15 (38°29'32.3"N 39°21'03.8"E)	0.26–0.33	Yes, sand boils	No	Sand boil samples were taken
Site 19 Battalgazi/Malatya (38°25'21.7"N 38°21'56.9"E)	0.08 (Site specific value for $V_{s30} = 350$ m/s)	No	Yes SK13 5.53 km	
Site 22 Battalgazi/Malatya (38°28'38.6"N 38°23'26.4"E)	0.05–0.09	No	No	Surface geology is composed of high plasticity clays and ground was frozen

Table 2 (continued)

Site Name (coordinates)	Median PGA (g) based on possible V_{S30}	Surface manifestation of liquefaction	Borelog available (proximity to the site)	Remark
Site 26 Kale/Malatya (38°25′25.1″N 38°45′46.1″E)	0.11–0.18	Yes, sand boils	No	Sand boil samples were taken
Site 28 Abdullah Pasa/Elazig (38°39′29.8″N 39°08′58.4″E)	0.13 (site specific value for V_{S30} = 350 m/s) 0.09 (site specific value for V_{S30} = 900 m/s)	No	No	
Site 30 Sursuru/Elazig (38°40′03.9″N 39°1′14.8″E)	0.13 (site specific value for V_{S30} = 375 m/s)	No	No	
Site 32 Mustafa Pasa/Elazig (38°40′15.9″N 39°13′59.9″E)	0.142 (site specific value for V_{S30} = 325 m/s)	No	Yes	SK142 (0.32 km) SK141 (0.90 km) SK183 (1.66 km) SK119 3.31 km
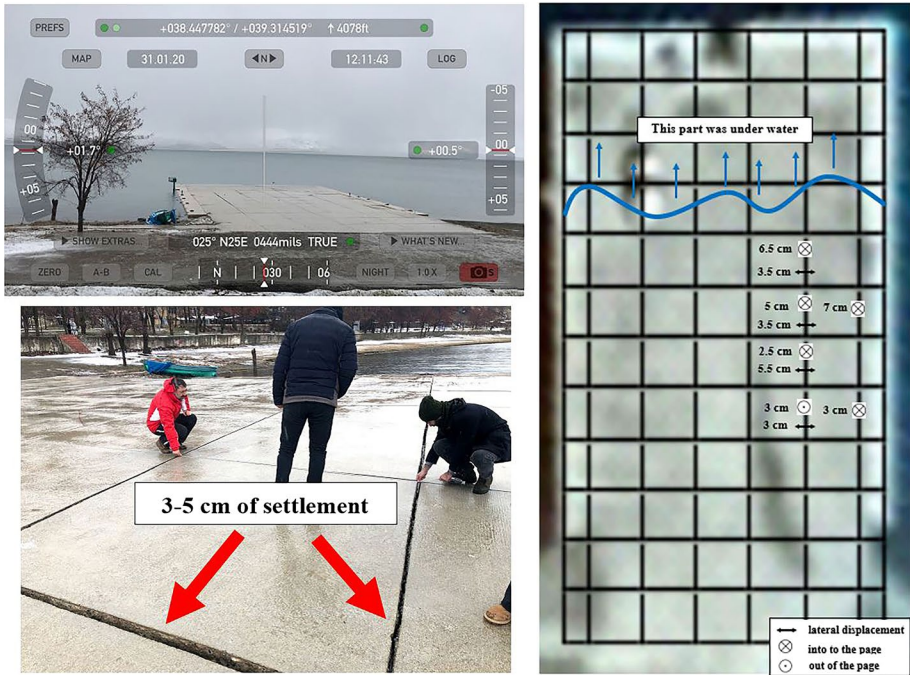
Fig. 5 Seismically-induced volumetric settlement in the dock of Lake Hazar (38°28′10.0″N 39°17′03.6″E/31.01.2020/12:11 & 38°26′53.2″N 39°18′53.4″E/31.01.2020/12:14)

Fig. 6 Seismically-induced lateral spreading on the beach of Lake Hazar (38°26′50.7″N 39°18′56.9″E/31.01.2020/12:21)
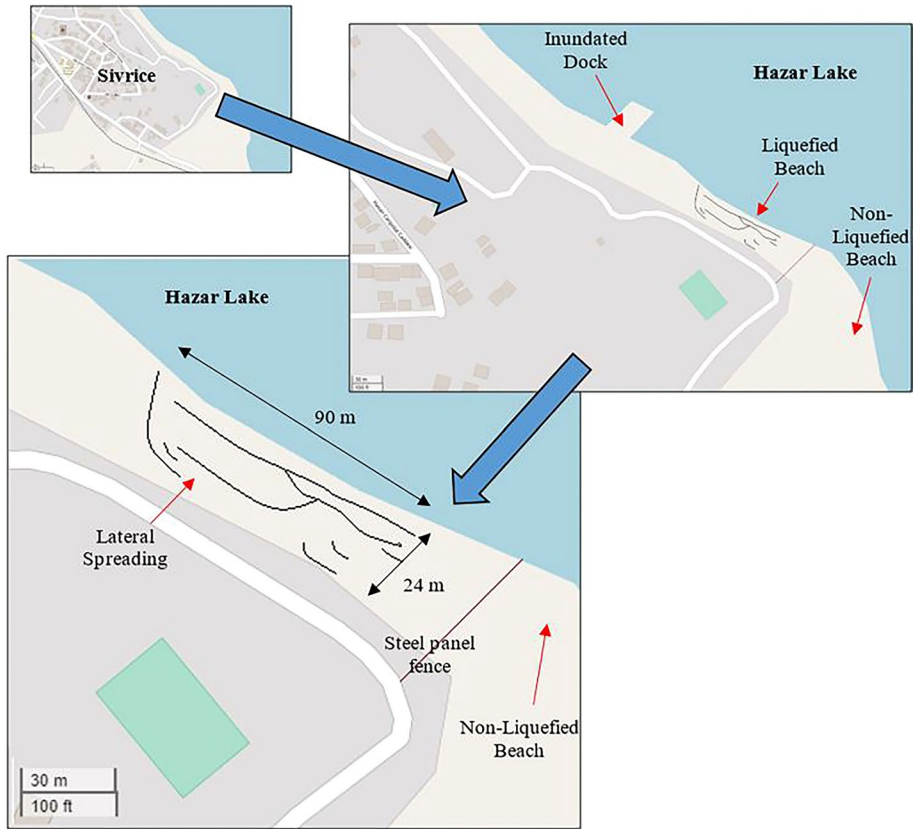
Fig. 7 A sketch of lateral spread deformations (38°28′10.0″N 39°17′03.6″E/31.01.2020/12:11), Google Maps, 2020

Seismically-induced liquefaction manifestations in the form of sand boils were observed at Site 8, Site 12, and Site 15, as shown in Figs. 8, 9 and 10. Soil samples were retrieved to perform sieve analysis at Middle East Technical University Soil Mechanics Laboratory. The resulting gradation curves for the samples collected from sand boils are presented later in this manuscript.

Sivrice–Elazig event also shook Malatya Downtown and its surrounding towns. Toygar Neighborhood of Battalgazi District was visited during the reconnaissance study. Although this site is composed of alluvial deposits with potential for ground failure, no signs of it were observed. Surficial soils, observed to be of high plasticity clays, and to be frozen are listed as the two factors, which might have impeded the development of permanent ground deformations or cyclic mobility manifestations. Seismically-induced liquefaction manifestations were observed at Kale District shore, in the form of sand boils. Figures 11 and 12 illustrate a view of the site and sand boils documented. Soil samples were collected for sieve analysis.

Fig. 8 Sand boils observed at Site 8 (38°27′49.7″N 39°24′01.1″E/31.01.2020/14:38 & 38°27′49.8″N 39°24′03.0″E/31.01.2020/14:14)

Fig. 9 Sand boils observed at Site 12 (38°29′58.5″N 39°30′24.6″E/31.01.2020/15:29 & 38°29′57.7″N 39°30′24.0″E/31.01.2020/15:30)

Fig. 10 Seismic soil liquefaction-induced sand boils at Site 15 (38°29′32.3″N 39°21′03.8″E/31.01.2020/16:57 & 38°29′34.5″N 39°21′03.6″E/31.01.2020/17:11)

Fig. 11 View of Kale shore (38°25′22.2″N 38°45′40.9″E/01.02.2020/12:17)

2.2 Preliminary liquefaction triggering assessments

In this section, on the basis of available sand ejecta samples, liquefaction susceptibility assessments of liquefied soil layers will be discussed. When representative in-situ field test results are available, in the form of SPT (standard penetration test), CPT (cone penetration test) or V_s (shear wave velocity), liquefaction triggering assessments on the basis of simplified procedures were performed, which will be discussed next.

Fig. 12 Seismic soil liquefaction-induced sand boils at Kale shore (38°25′15.2″N 38°45′32.2″E/01.02.2020/12:32 & 38°25′15.2″N 38°45′23.9″E/01.02.2020/12:45)

2.2.1 Liquefaction susceptibility assessments

As stated earlier, disturbed samples were retrieved from soil ejecta at various sites. These samples were tested in conformance with ASTM D7928-17 and ASTM D6913/D6319M-17 standards to assess grain size distribution characteristics, and to classify them. The locations of sites, and grain size distribution characteristics are summarized in Table 3. In Fig. 13, grain size distribution curves are also comparatively presented with the range of potentially liquefiable soils (Tsuchida 1970). Based on Unified Soil Classification System (USCS) (ASTM D2487-17e1), most of the sand ejecta samples were classified as SP (poorly graded sand) and SM (silty sand) and fall in the range of potentially liquefiable soils. Consistent with available literature, ejecta materials were classified as non-plastic with fines less than 30%.

2.2.2 Likelihood of liquefaction triggering

Due to reconnaissance nature of the studies and lack of site-specific investigation results, available nearby borelogs from local site investigation database catalogs (M. Gor, personal communication, 2020) of Elazig and Malatya were compiled and assessed to perform preliminary liquefaction triggering analysis. As discussed earlier, plastic cohesive soil layers dominate the alluvial geological setting of Elazig and Malatya Downtowns. Figure 14 represents the consistency limits of samples taken from Elazig and Malatya Downtown, and Lake Hazar. Therefore, the number of potentially liquefiable sites and soil layers are limited; and they did not liquefy during this event. Figure 15

Table 3 Grain size distribution of sand ejecta

Region	Coordinates (x–y)	Gravel (%)	Sand (%)	Fines (%)	Silt (%)	Clay (%)	D_{10} (mm)	D_{30} (mm)	D_{60} (mm)	C_U[a]	C_C[a]	Soil type
Lake Hazar	38.463–39.4009 (Site-8)	11.0	87.6	1.4			0.33	0.42	0.53	1.61	1.01	SP
	38.463–39.4007 (Site-8)	28.8	41.1	30.1	27.6	2.5	0.02	0.075	0.6	30.0	0.47	SM
	38.463–39.4002 (Site-8)	4.2	72.7	23.1	19.6	3.5	0.03	0.09	0.17	5.67	1.59	SM
	38.499–39.506 (Site-12)	4.2	80.9	14.9	11.1	3.8	0.02	0.24	0.42	21.0	6.86	SM
	38.492–39.35 (Site-15)	10.0	87.0	3.0			0.32	0.65	1.7	5.31	0.78	SP
	38.492–39.351 (Site-15)	4.1	83.5	12.5	10.6	1.9	0.06	0.16	0.25	4.17	1.71	SM
Kale District shore	38.424–38.762 (Site-26)	36.4	57.5	6.2			0.09	0.2	2.9	32.2	0.15	SP–SM
	38.421–38.759 (Site-26)	3.4	95.4	1.3			0.23	0.36	0.49	2.13	1.15	SP
	38.421–38.757 (Site-26)	4.4	90.4	5.2			0.25	0.47	0.91	3.64	0.97	SP–SM
	38.424–38.762 (Site-26)	26.2	70.8	3.0			0.32	0.5	1.44	4.50	0.54	SP

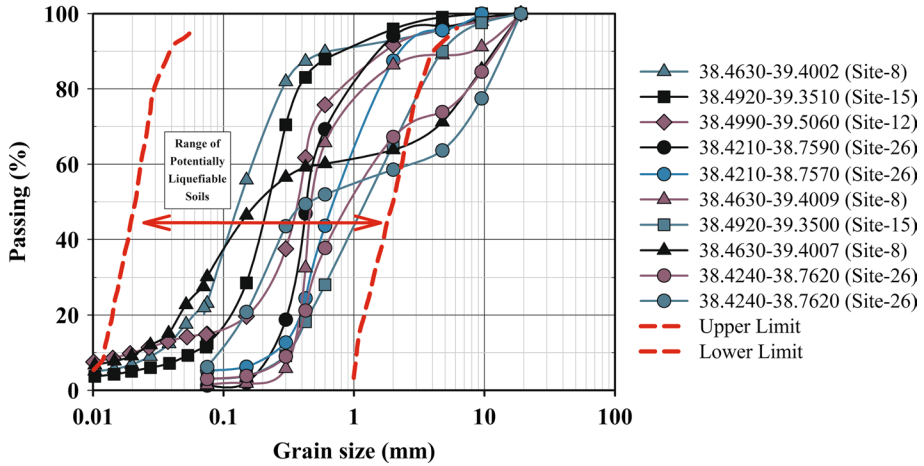[a]$C_u = D_{60}/D_{10}$, $Cc = D_{30}^2/(D_{10} * D_{60})$

Fig. 13 Particles size distribution curves of the sand ejecta retrieved from liquefied sites
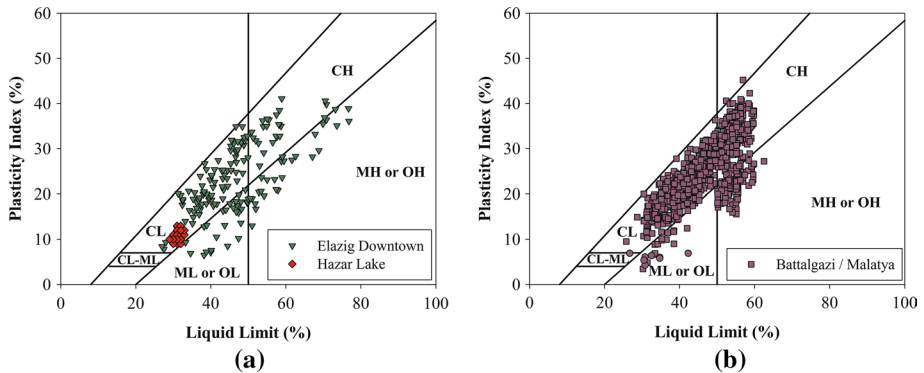

Fig. 14 Local fine grained soil on the plasticity chart (ASTM D2487-17e1)

presents representative borelogs with potentially liquefiable critical soil layers. In the same figure, the coordinates of the borelogs were given with available soil stratigraphy and overburden, equipment and procedure corrected SPT $N_{1,60}$ values. Potentially liquefiable soil layers are defined as sand layers and/or non-plastic to low plasticity (less than 7%) fine soil layers.

CSR values were estimated closely following the simplified procedures (Seed and Idriss 1971) along with the protocols defined by Cetin et al. (2018). The site specific PGA values were estimated as 0.09–0.10, 0.13, 0.27 g for Malatya and Elazig Downtown, and Lake Hazar sites, respectively. Table 4 presents a summary of liquefaction assessment results.

Figure 16 presents the findings shown on Cetin et al. (2018) liquefaction triggering correlations. The site performances were observed to be consistent with the predictions of triggering relationships. Elazig and Malatya–Battalgazi cases were judged to be non-informative non-liquefaction cases (i.e.: cases where liquefaction triggering probabilities P_L are very low; i.e.: < 1%) whereas Lake Hazar cases fall within the boundary of liquefied and non-liquefied zones, in conformance with the overall marginal liquefaction responses
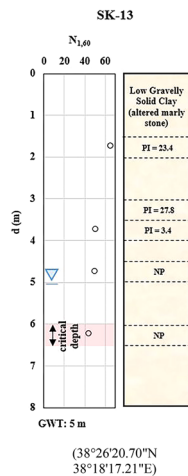
Fig. 15 Available representative borelogs from **a** Elazig **b** Lake Hazar and **c** Malatya
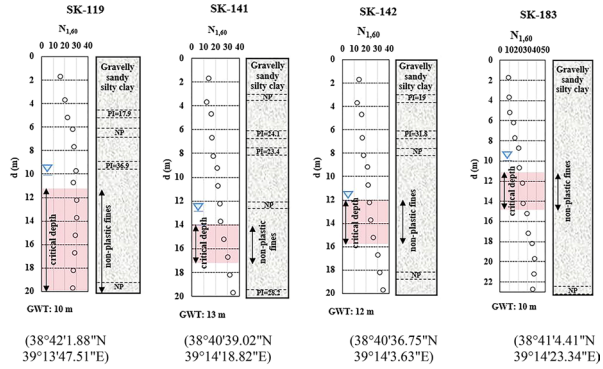

(a) Elazig Downtown
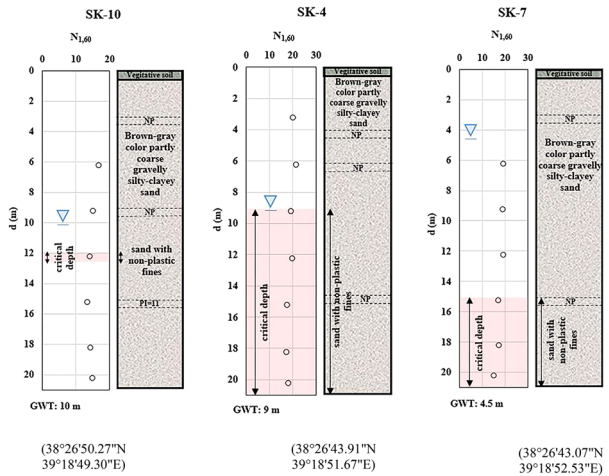
(b) Lake Hazar

(c) Battalgazi / Malatya

Table 4 Summary of the liquefaction assessment (M=6.8; K_M=1.256; C_s=1; C_B=1; C_E=0.75)

Site	Liq.?	$d_{crt.}$ (m)	GWT (m)	σ_v (kPa)	σ_v' (kPa)	a_{max} (g)	V_{SI2} (m/s)	r_d	$CSR_{\sigma v,M}$	K_σ	$CSR_{\sigma v=1\,atm,\,M=7.5}$	FC (%)	N (mean)	C_R	C_N	$N_{1,60}$	$N_{1,60,CS}$	CRR $\sigma'v=1\,atm,\,M=7.5,\,PL=50\%$	P_L (%)	FS
SK-119	No	15.2	10.0	284	233	0.13	250	0.878	0.092	0.8	0.097	–	58	1.0	0.7	29	29.39	0.138	<1	1.27
SK-141	No	15.2	13.0	283	261	0.13	250	0.878	0.081	0.7	0.089	–	53	1.0	0.6	24	25.07	0.120	<1	1.24
SK-142	No	13.7	12.0	241	224	0.13	250	0.905	0.083	0.8	0.087	40.6	45	1.0	0.7	23	27.15	0.078	<1	0.80
SK-183	No	12.5	10.0	229	204	0.13	250	0.927	0.089	0.8	0.090	–	46	1.0	0.7	24	24.96	0.131	<1	1.25
SK-10	Yes	12.2	10.0	225	203	0.27	295	0.988	0.191	0.8	0.193	50.0	27	1.0	0.7	14	18.16	0.166	48	0.74
SK-4	Yes	15.2	9.0	285	224	0.27	295	0.973	0.217	0.8	0.226	42.2	37	1.0	0.7	19	22.75	0.201	24	0.80
SK-7	Yes	15.2	4.5	295	189	0.27	295	0.973	0.265	0.8	0.261	37.1	36	1.0	0.7	19	23.69	0.259	41	0.84
SK-13	No	6.2	5.0	113	101	0.10	292	0.999	0.071	1.0	0.057	24.6	60	0.95	1.0	43	46.55	0.071	<1	0.91

Fig. 16 Liquefaction triggering assessment results as compared with the database of Cetin et al. (2018)
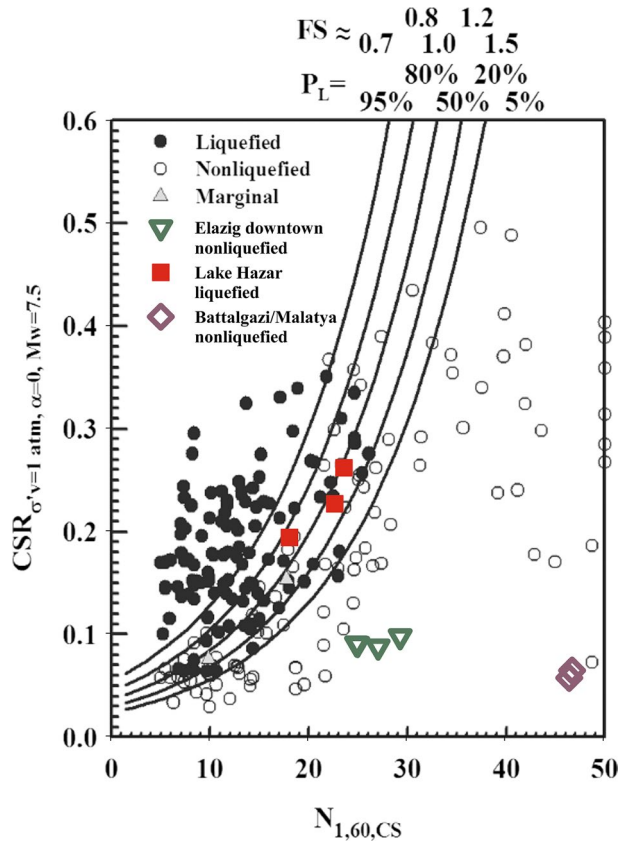
observed along the coast of the lake. Hence, these cases will be valuable in the development of future case-history based liquefaction triggering relationships.

3 Performance of slopes

A number of natural and engineered soil and rock slopes was also visited, the performance of which were documented in Table 5. Figures 17, 18 and 19 present sample views of soil and rock slopes with and without failure.

Rock falls were mapped at a site located near northern shores of Lake Hazar, as shown in Fig. 20. At this site, the surface geology is composed of Phyllites with schistocity texture. The cross section is estimated as 15 m—high with a slope of 50°. The dimensions of the some fallen rock blocks and the distance of these blocks to the toe of the upper bench were measured in the field, as summarized in Table 6. No fallen blocks were observed on the lower, second bench of the highway cut. Slope angle, length and height of different sections of the upper and lower benches, and possible heights where rock falls were initiated from, were also mapped in the field.

A series of rockfall analysis was performed. Rocscience-RocFall 2019 software was used to estimate the initial velocity of the fallen rock blocks. Figure 21 presents a

Table 5 Summary of soil and rock slope sites

Site name (coordinates)	Median PGA (g) based on possible V_{S30}	Slope material	Slope height/angle	Remark
Site 5 (38°26′43.7″N 39°20′40.7″E)	0.37–0.39	Neritic limestone	5–6 m high/~ 45°	No failure
Site 7 (38°27′31.0″N 39°22′55.9″E)	0.27–0.34	Neritic limestone	5–6 m high/> 45°	No failure
Site 10 (38°28′52.6″N 39°27′16.9″E)	0.16–0.25	Continental clastic rocks	5–6 m high/~ 45°	No failure
Site 13 (38°31′40.3″N 39°28′02.9″E)	0.14–0.22	Phyllites with schistocity texture	15 m high/~ 50°	Rockfalls were mapped
Site 14a (38°30′11.7″N 39°23′33.4″E)	0.196–0.28	Mesozoic undifferentiated basic and ultrabasic rocks formations	~ 65°	No failure
Site 14b (38°30′11.4″N 39°23′34.9″E)	0.20–0.28	Neritic limestone	~ 39°	Fallen rock blocks were observed. The approximate diameters of the fallen rock blocks vary from 80 to 120 cm
Site 17 (38°26′19.8″N 38°49′38.8″E)	0.12–0.20	Clastic and carbonate rocks		2–3 m diameter rock blocks were fallen freshly on the shoulders of the highway
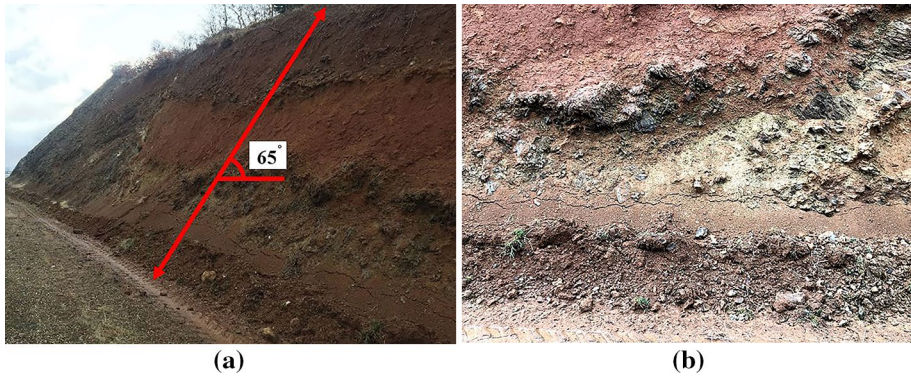
Figure 17 a Side view of Site 14 the slope 65° (38°30′11.7″N 39°23′33.4″E/31.01.2020/16:34), and **b** interlayering at rock formation (38°30′11.8″N 39°23′33.3″E/31.01.2020/16:34)

Fig. 18 Rock falls at Site 14 (38°30′11.4″N 39°23′34.9″E/31.01.2020/16:37 & 38°30′11.3″N 39°23′34.7″E/31.01.2020/16:37)

sample of these back analyses. These simulations suggested a peak ground velocity of 4–6 m/s at the site to produce comparable rock fall paths. Comparably, the peak ground velocity (PGV) at this site was estimated to fall in the range of 5–19 m/s by ASK14.

Fig. 19 Fallen rock blocks on the highway bench (38°26′19.8″N 38°49′38.8″E/01.02.2020/7:23)

4 Performance of hydraulic structures

Immediately after the event, two reconnaissance teams from General Directorate of State Hydraulics Works (DSI) and METU-Civil Engineering Department inspected six of the hydraulic dams, which were constructed for energy generation and irrigation purposes along Euphrates basin. Figure 4 presents the locations of these dams and strong ground motion stations.

The major characteristics of these dams are summarized in Table 7, along with a summary of their seismic performance. The field reconnaissance observations are merely descriptive in nature, and discussions (and assessments) regarding the mechanisms of seismically-induced ground deformations (or lack of these deformations) are excluded from the scope of this manuscript due to reconnaissance nature of the field studies.

4.1 Dedeyolu Dam

Dedeyolu Dam is a 35.7-m-high, earthfill dam, built on Kumardi River within the borders of Elazig province. The construction of the dam was completed in between the years of 1999–2006. The dam serves to fulfill the irrigation needs of 0.41 ha croplands. It is
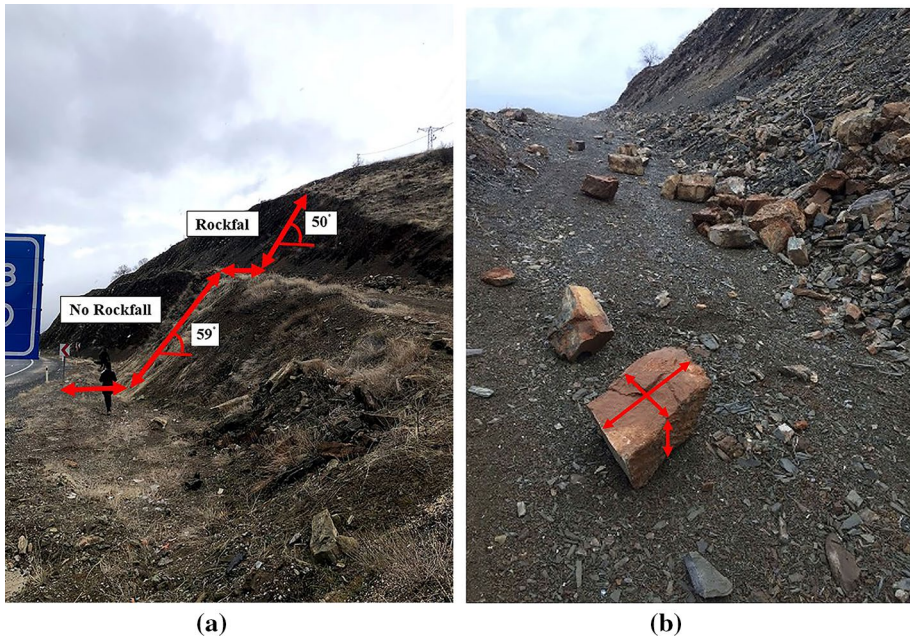
Fig. 20 Rockfalls site **a** general view (38°31′40.3″N 39°28′02.9″E/31.01.2020/16:20), **b** fallen rocks (38°31′41.0″N 39°27′59.6″E/31.01.2020/16:13)

**Table 6** Dimensions of fallen rock blocks at Site 13

Length (cm)	Height (cm)	Width (cm)	Distance of the rock blocks to the toe of the slope (m)
60	30	35	3.9
32	15	30	5
55	30	28	3.2

founded on mostly Pliocene-age stiff clay underlain by cretaceous diabase. General layout and typical cross section of the dam are presented in Fig. 22a, b, respectively.

Dedeyolu Dam is located approximately 19.3 km north-east of Sivrice earthquake epicenter. Peak rock ground acceleration ($PGA_{VS30=1100 \text{ m/s}}$) is estimated as ~ 0.23 g. The PGA on a nearby stiff clayey soil site with an approximate V_{S30} value of 350 m/s is estimated as ~ 0.32 g (Fig. 3b).

DSI reconnaissance team has investigated the dam and documented 3–8 mm wide, minor longitudinal surface cracks along the crest road, as shown in Fig. 22c. A few test pits were opened, which confirmed the limited extent of crack to clay core. Even though Dedeyolu Dam was tested by higher levels than the design basis event ($PGA_{design} \approx 0.2$ g), the performance of it was observed to be satisfactory.

With the intent of comparatively assessing the measured permanent deformations with the ones predicted by Makdisi and Seed (1977), the recommended procedure is closely followed as illustrated in Fig. 23. The critical failure surfaces were estimated separately for upstream and downstream sections, through series of limit equilibrium assessments, which
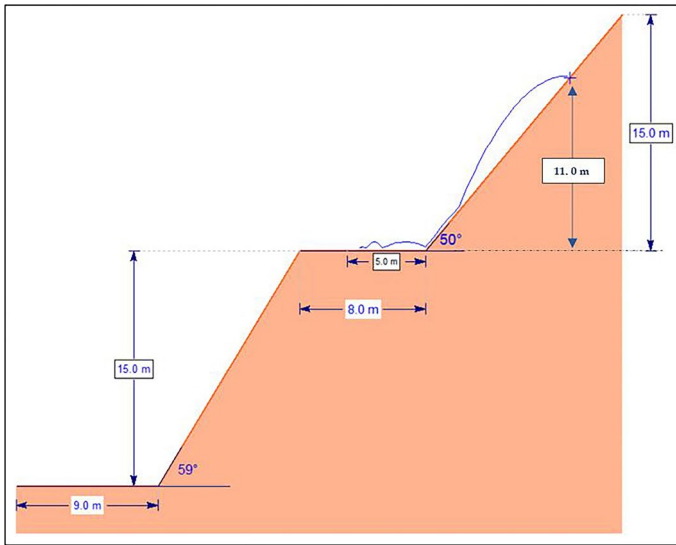
Fig. 21 A sample back analysis of rockfall cases with RocFall 2019 software

were determined to pass through the toes of the dam. The shear strength parameters for the clay core (high plasticity clay, CH) and semi-pervious zone (silty–clayey sand, SM–SC) were preliminarily used as $c' = 15$ kPa & $\phi' = 24°$ and $c' = 5$ kPa & $\phi' = 28°$, respectively, consistent with available field and laboratory test results. The natural period of the dam and crest accelerations were estimated as 0.27 s and 0.62 g on the basis of relationships proposed by Dakoulas and Gazetas (1985) and Kavruk (2003). As shown in Fig. 23, the permanent deformations by Makdisi and Seed (1977) procedure were estimated approximately 1 and 5 mm for the slip surfaces passing through the upstream and downstream toes, respectively, which were concluded to be in good agreement with the width of cracks observed in the crest. It should be noted that these assessments are preliminary in nature and more refined analyses are to be performed for improved evaluations.

4.2 Kapikaya Turgut Ozal Dam

Kapikaya Turgut Ozal Dam is an 89.5-m-high, rockfill dam with a central clay core, built on Mamikhan Stream within the borders of Malatya province. The construction of the dam was completed in between the years of 1998–2012. The dam was put into operation in 2012, and since then 3,662 ha land has been irrigated. The dam is founded on diabase. General layout and typical cross section of the dam are presented in Fig. 24a, b, respectively. Kapikaya Turgut Ozal Dam is located approximately 39.8 km west of Sivrice earthquake epicenter. Peak rock ground acceleration ($PGA_{VS30=1100 \text{ m/s}}$) is estimated as ~0.10 g (Fig. 3b). Design basis peak ground acceleration at the dam site was reported as 0.15 g.

   Reconnaissance team has investigated the dam and documented no signs of seismically induced permanent deformations along the dam crest. During site visit, the water level was measured at +854.70 m elevation. Both the upstream and downstream slopes along with the dam axis itself were documented to be unaffected from the shaking. Also, no damage

Table 7 Major characteristics of dams

	Dedeyolu Dam	Kapikaya Turgut Ozal Dam	Karakaya Dam	Cip Dam	Keban Dam	Boztepe Recai Kutan Dam
Location (District)	Elazig (Sivrice)	Malatya	Malatya–Diyarbakir Border	Elazig	Elazig	Malatya
Purpose	Irrigation	Irrigation	Energy	Irrigation	Energy/irrigation	Irrigation
Construction period (year)	1999–2006	1998–2012	1976–1987	1965–1965	1965–1974	1997–2002
Dam type	Clay core homogeneous earthfill dam	Clay core rockfill	Concrete arch	Earthfill	Clay core rockfill + concrete gravity	Clay core sand–gravel–rockfill
Dam volume (10^3 m^3)	721	4415	2000	446	15,585	6900
Height from foundation (m)	35.7	89.5	173.0	24.0	207.0	82.0
Total reservoir capacity (hm^3)	3.44	71.14	9580	7.00	31,000	116.10
Active storage (hm^3)	3.27	68.34	5,580	–	13,927	101
Reservoir area (km^2)	0.37	2805	28	1.1	675	5250
Distance from EQ epicenter (km)	19.3	39.8	16.1	35.5	56.6	87.6
R_{jb} (km)	8.3	22.5	14.4	33.5	58.5	76.3
PGA$_{VS30=1100 m/s}$ (g)[a]	0.225	0.102	0.150	0.070	0.038	0.027
Performance remarks	Note[b]	Note[c]	Note[d]	Note[c]	Note[e]	Note[c]

[a]Median estimations of ASK14 GMM

[b]Minor 3–8 mm wide, shallow longitudinal cracking along the crest

[c]No signs of permanent ground deformations

[d]A slight increase in discharge from drainage holes at +528 m elevation gallery. Traces of surface rupture and lines of water or gas extrusions observed at the reservoir. Reservoir observed to be muddy, following the few days of the main event

[e]No surface manifestation of ground deformations. Magnetic extensometers installed in the clay core, suggested a maximum of 2 cm vertical deformations
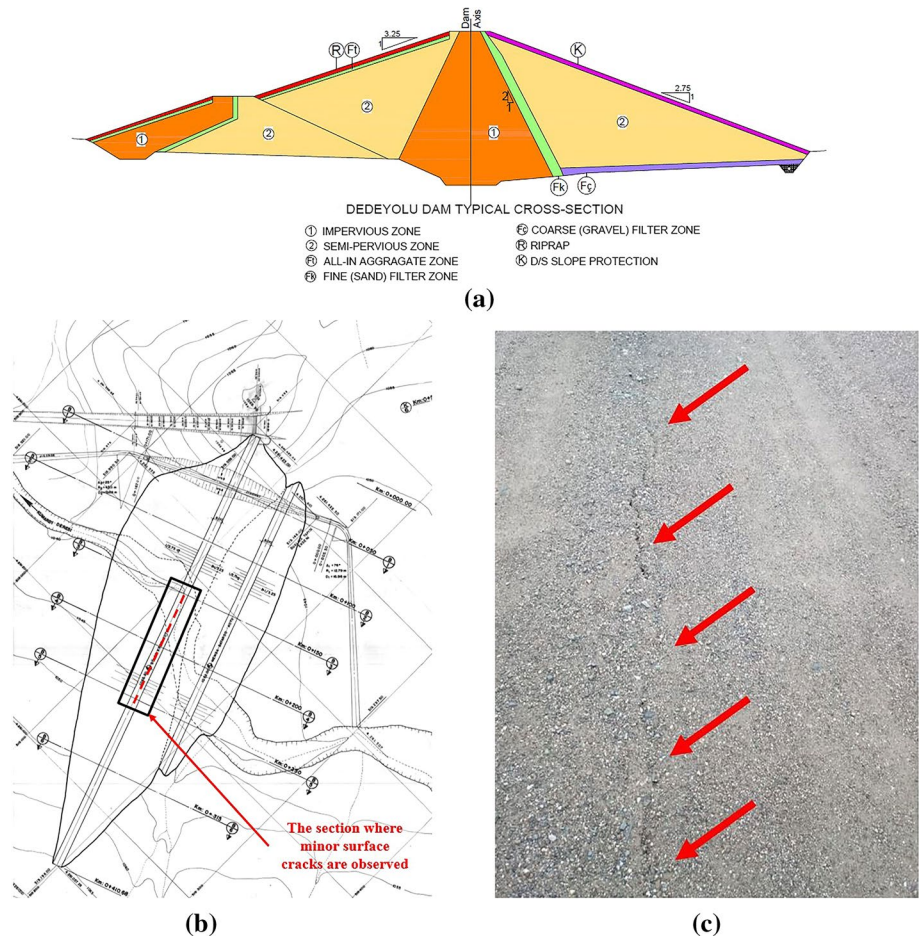
Fig. 22 **a** General layout of Dedeyolu Dam (Courtesy of DSI), **b** Typical cross section of Dedeyolu Dam (after DSI), **c** minor, 3–8 mm wide, longitudinal cracks along the crest of Dedeyolu Dam (Courtesy of DSI)

of water in-take and spillway were observed. Pictures taken at the dam site during the field study of METU reconnaissance team are given in Fig. 25a, b.

4.3 Karakaya Dam

Karakaya Dam is a 173-m-high, concrete arch dam, built on Euphrates River within the borders of Diyarbakir–Malatya provinces. The construction of the dam was completed in between the years of 1976–1987. The dam was put into operation in 1987, and since then annually 7354 GWh. hydro-electric power has been produced. The dam is founded on horn-blende-gneiss massive rock complex. Therefore, the location of the dam site benefits from the advantages of favorable topography and hard and massive foundation rock type. General layout and typical cross section of the dam are presented in Fig. 26a, b, respectively.

(a)

(b)

(c)
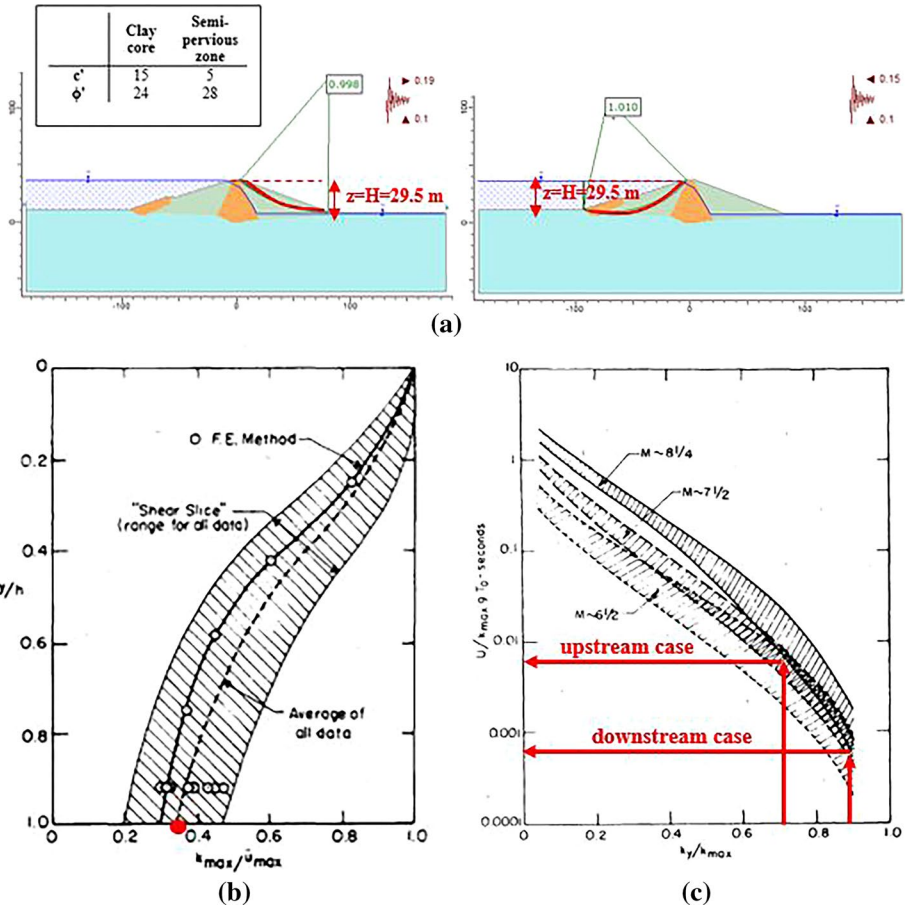
Fig. 23 **a** Limit equilibrium-based slope stability models for Dedeyolu Dam, **b** maximum acceleration ratio of Dedeyolu Dam, **c** normalized permanent displacement estimated for Dedeyolu Dam
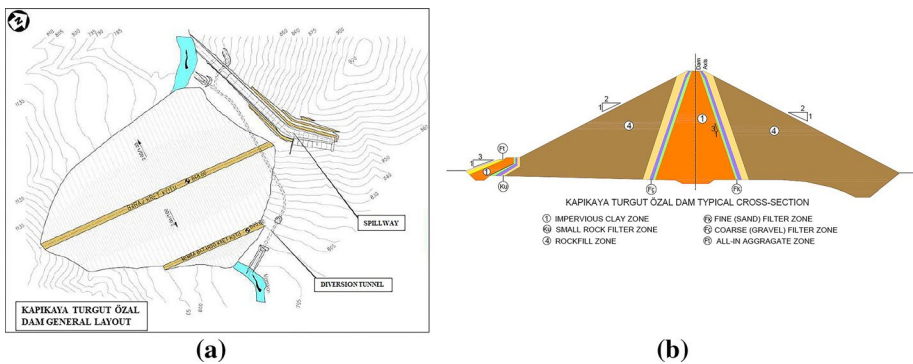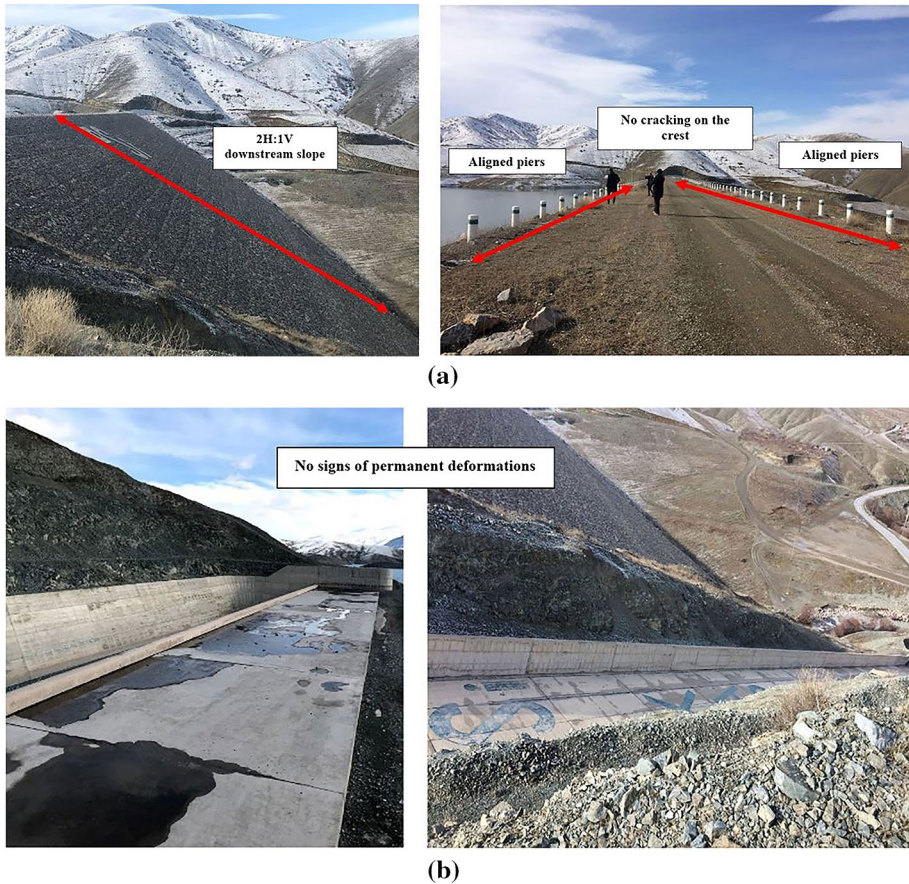

(a)

(b)

Fig. 24 **a** General layout of Kapikaya Turgut Ozal Dam (Courtesy of DSI), **b** typical cross section of Kapikaya Turgut Ozal Dam (after DSI)

(a)

(b)

Fig. 25 **a** Side and crest view of Kapikaya Turgut Ozal Dam, **b** water in-take structure and spillway of Kapikaya Turgut Ozal Dam

Karakaya Dam is located approximately 16 km south of Sivrice Earthquake epicenter. Peak rock ground acceleration ($PGA_{VS30=1100 \text{ m/s}}$) is estimated as ~0.15 g (Fig. 3b).

DSI reconnaissance team documented no signs of seismically induced permanent deformations along the dam crest and inside the galleries. Spillway gates were opened and closed with no problem, which have confirmed their elastic response during and after the event. A slight increase in water discharge from drainage holes at +528 m elevation gallery. The discharge was reported as 127.4 lt/min. measured after the event. Additionally, MTA (General Directorate of Mineral Research and Exploration) reconnaissance team observations from Karakaya Dam reservoir revealed some traces of surface rupture and lines of water or gas extrusions crossing the dam reservoir. Figure 27 presents a view of the water or gas bubbles. Also, Karakaya Dam hydropower plant staff has reported that dam reservoir was observed to be muddy, following the few days of the main event.
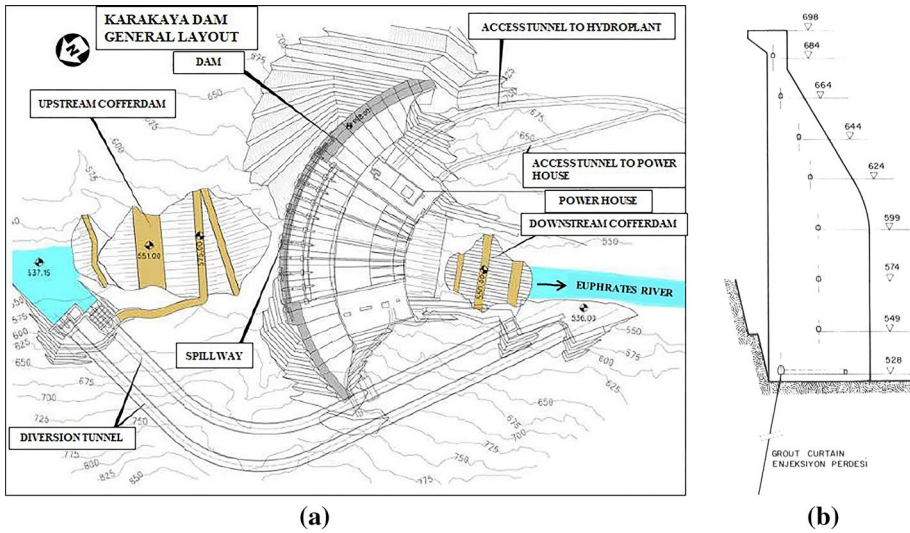
Fig. 26 a The general layout of Karakaya Dam (Courtesy of DSI), **b** Typical cross-section of Karakaya Dam (Courtesy of DSI)
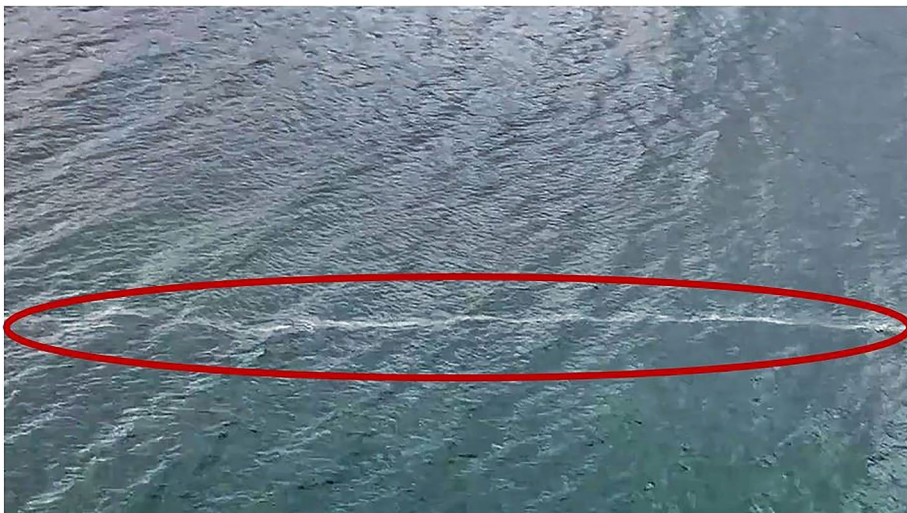
Fig. 27 Gas and water bubles along the fault trace observed crossing Karakaya Dam reservoir (Courtesy of Anadolu Agency)

4.4 Keban Dam

Keban Dam is a 207 m-high, combined rockfill and concrete gravity dam with a central clay core, built on Euphrates River within the borders of Elazig province. The construction of the dam was completed in between the years of 1965–1974. The dam was put into operation in 1974, and since then annually 6,000 GWh. hydro-electric power has been
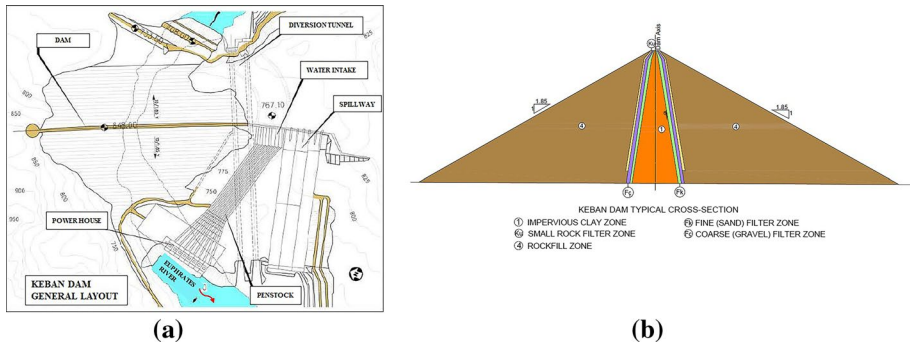
Fig. 28 **a** General layout of Keban Dam (Courtesy of DSI), **b** Typical cross section of Keban Dam (after DSI)

produced. The dam is founded on medium to thick, bedded limestone and dolomite which are grey, black and riverbed beige in color, massive and hard in texture. General layout and typical cross section of the dam are presented in Fig. 28a, b, respectively. Keban Dam is located approximately 56.6 km north-west of the epicenter. Peak rock ground acceleration ($PGA_{VS30=1100 \text{ m/s}}$) is estimated as ~ 0.04 g (Fig. 3b).

Consistent with the low level of shaking, DSI reconnaissance team has documented no signs of seismically induced permanent deformations along the dam crest and inside the cut-off galleries. No surface manifestation of ground deformations was detected; however, magnetic extensometers installed in the clay core, suggested a maximum of 2 cm vertical deformations (settlements) after the earthquake. Spillway gates were opened and closed with no problem, which have confirmed their elastic response and functionality during and after the event. Keban Dam has demonstrated a satisfactory response during and after this event.

5 Performance of residential building foundations

Field investigation studies have also covered heavily affected Elazig and Malatya city centers. Damages on a number of non-engineered masonry, and reinforced concrete structures were observed. Some of these structures suffered from intensive cracking, partial collapse, whereas some others experienced no evident damage. The discussion of these non-geotechnical issues is not within the scope of this manuscript, and readers are referred to Cetin et al. (2020) and METU EERC (2020) for in depth discussion of these structural damages. However, foundation performances of these buildings will be briefly discussed for documentation purposes in Table 8.
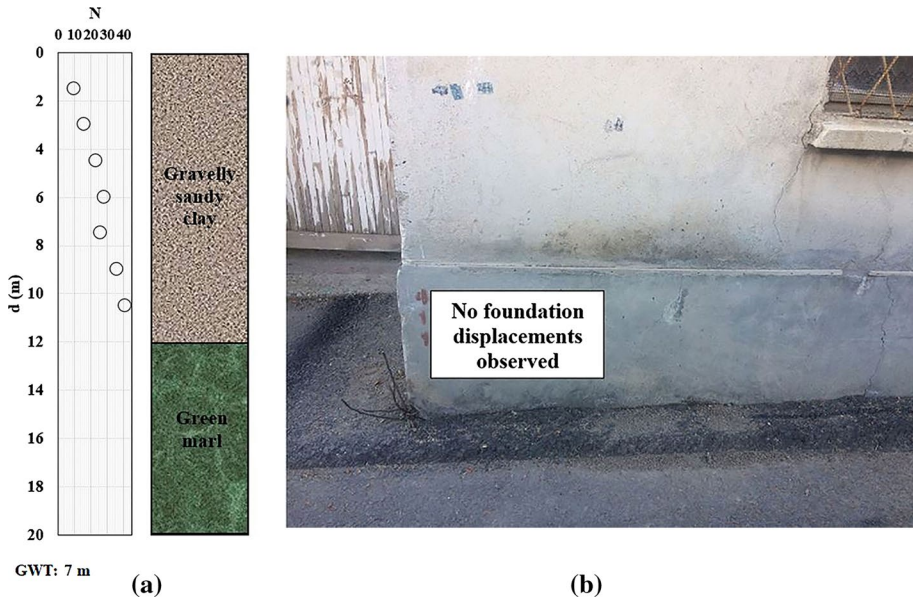
5.1 Battalgazi/Malatya

Plio-Quaternary aged lake sediments dominate the soil profile in Battalgazi. The upper surficial layers up to depth range of 8–12 m, are classified as gravelly sandy clay, which are underlain by green marl. Groundwater table is located in between depth range of 4 to 10 m. A representative lithology is presented in Fig. 29a. V_{S30} for the area is measured in the range of 300–400 m/s by Multi-Channel Surface Wave Analysis Method (MASW). As

Table 8 Summary of the performance of residential building foundations

| Site name (coordinates)	Median PGA (g) based on possible V_{S30}	Remark
Site 19—Battalgazi/Malatya (38°25′20.7″N 38°21′59.3″E)	0.081 (for V_{S30} = 350 m/s)	No signs of permanent foundation displacements of R/C buildings
Site 28—Abdullah Pasa/Elazig (38°39′21.9″N 39°09′10.4″E)	0.130 (for V_{S30} = 350 m/s) 0.09 (for V_{S30} = 900 m/s)	1–2 cm settlements, cracking of the residential buildings' entrance stairs, and no signs of permanent foundation deformations
Site 30—Sursuru/Elazig (38°40′03.9″N 39°11′14.8″E)	0.130 (for V_{S30} = 375 m/s)	None to 1–13 cm foundation settlements
Site 32—Mustafa Pasa/Elazig (38°40′03.9″N 39°11′14.8″E)	0.142 (for V_{S30} = 325 m/s)	No signs of permanent foundation displacements of R/C buildings

Fig. 29 **a** Typical borelog for Malatya-Battalgazi (M. Gor, personal communication 2020), **b** An example of no foundation displacements observed at a residential R/C building in Battalgazi (38°25′20.7″N 38°21′59.3″E/01.02.2020/8:31)

shown in Fig. 29b, no signs of permanent foundation displacements of R/C buildings were mapped in Battalgazi. The foundation systems are reported to be shallow individual footings combined with strap beams.

5.2 Abdullah Pasa District/Elazig

Abdullah Pasa District is one of the oldest residential districts of Elazig, where in the north limestone outcrops and dominates the rock profile with groundwater table to be located below 20 m depths. In this northern section V_{S30} is estimated to be greater than 800–1100 m/s. In other parts of the District, Plio-Quaternary aged young sediments dominate soil profiles. The upper surficial layers are classified as brown fine-gravelly, sandy silty clay. Gravels are reported to be magmatic origin. Groundwater table is located in the depth range of 10–14 m. A representative lithology is presented in Fig. 30. V_{S30} for the region is measured as 300–375 m/s by MASW.

A number of structurally damaged residential buildings was documented in Abdullah Pasa District of Elazig city center. The level of damage varies in a wide scale: from no damage to heavy damage. As shown in Figs. 31 and S1–S3 (given as part of the electronic supplement), foundation performances documented in this district vary from 1 to 2 cm settlements, and cracking of the residential buildings' entrance stairs, to no signs of permanent foundation deformations.
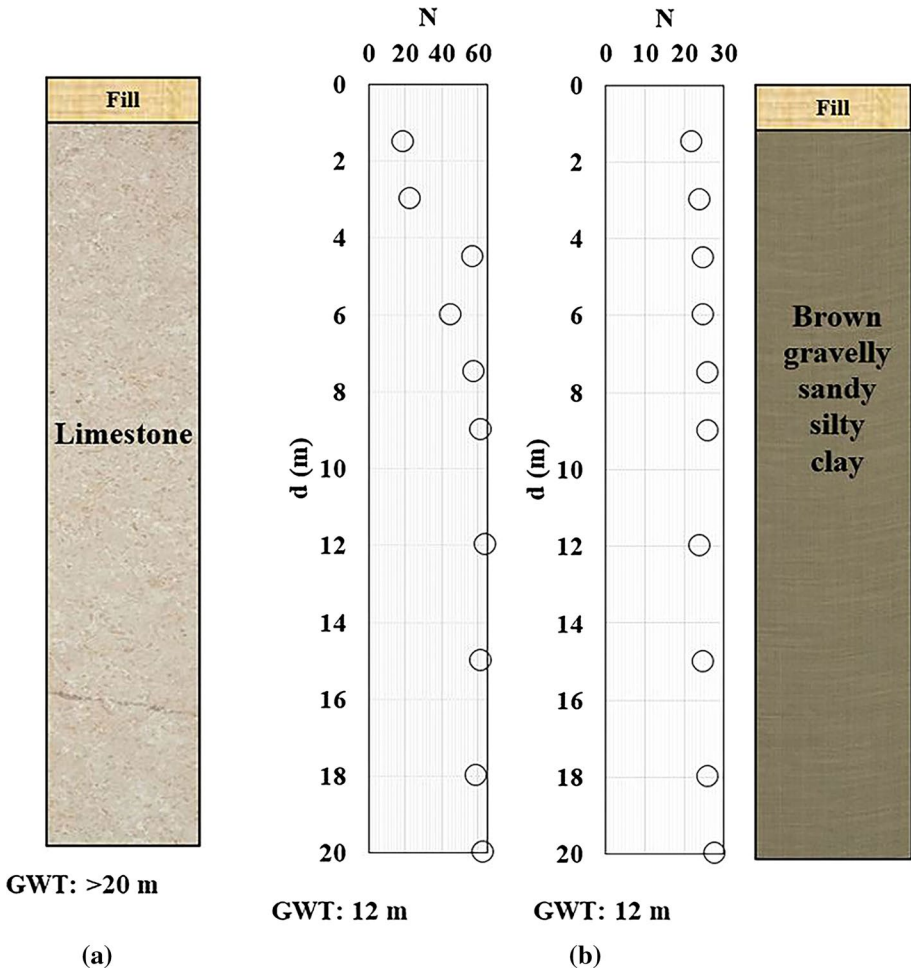
Fig. 30 Typical borelogs for Elazig-Abdullah Pasa District: **a** northern part, **b** other parts (M. Gor, personal communication 2020)
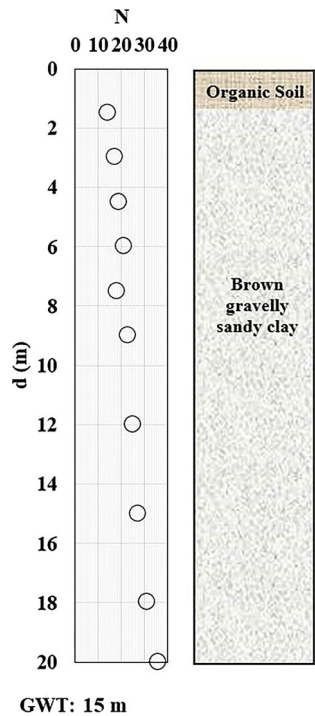
5.3 Sursuru District/Elazig

In the city of Elazig, most of the structural damage had been concentrated in Sursuru District, where Plio-Quaternary young sediments dominate soil profiles. The upper surficial layers are classified as brown gravelly sandy clay. A representative lithology is presented in Fig. 32. V_{S30} for the region was measured as 350–400 m/s by MASW. During the site visit, a field investigation study including borehole drilling, undisturbed and disturbed soil sampling with SPT measurements, was witnessed as shown in Fig. 33a. The borelog is retrieved by personal communication and is presented in Fig. 33b. A relatively undisturbed soil sample was taken from the borehole for further laboratory testing.

Oedometer tests were performed on this undisturbed sample retrieved at 9.5 m depth following ASTM D2435/D2435M-11 standards. The results are given in Fig. 34, confirming slightly overconsolidated (OCR = 2–3) and compressible nature of Sursuru District

Fig. 31 Cracking of entrance pavement due to seismically-induced lateral displacements observed at the entrance of the of a residential building (38°39′21.9″N 39°09′10.4″E/01.02.2020/14:50)

Fig. 32 Typical borelog for Elazig-Sursuru District (M. Gor, personal communication 2020)
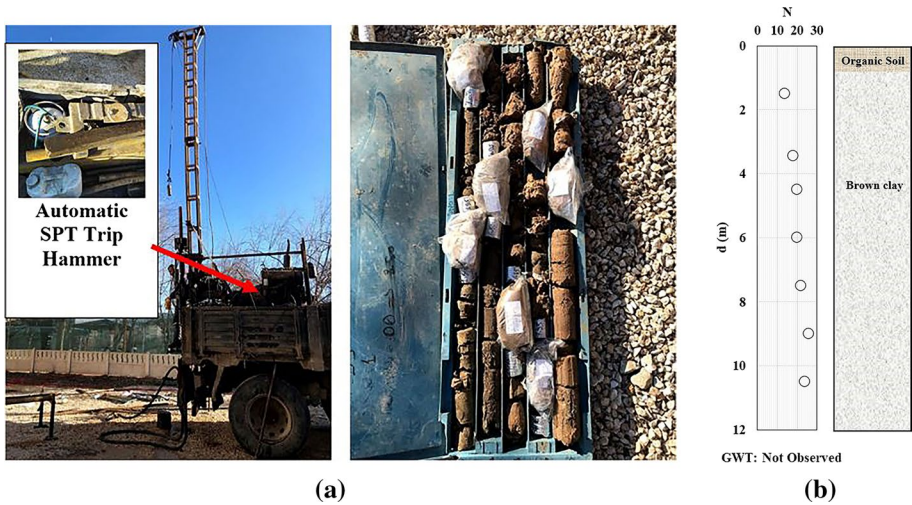
Fig. 33 a Drilling efforts (38°40′03.9″N 39°11′14.8″E/01.02.2020/15:18 & 38°40′03.1″N 39°11′16.1″E/01.02.2020/15:18), **b** the borelog of the witnessed site investigation at Sursuru District (38°40′03.9″N 39°11′14.8″E)
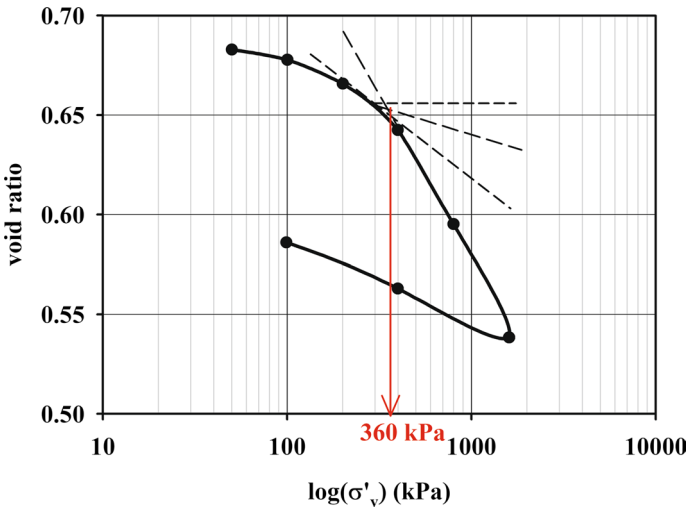
Fig. 34 Oedometer test results

clayey soils. Pre-consolidation pressure (σ'_p), recompression index (C_r) and compression index (C_c) were calculated as 360 kPa 0.038 and 0.156, respectively.

As shown in Figs. 35 and S4–S5 (given as part of the electronic supplement), the reconnaissance studies documented none to 1–13 cm foundation settlements. In Fig. 35,
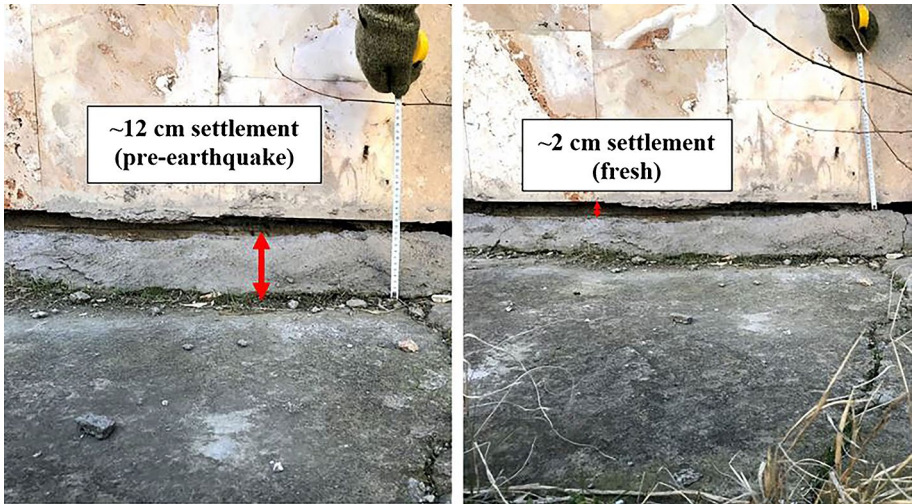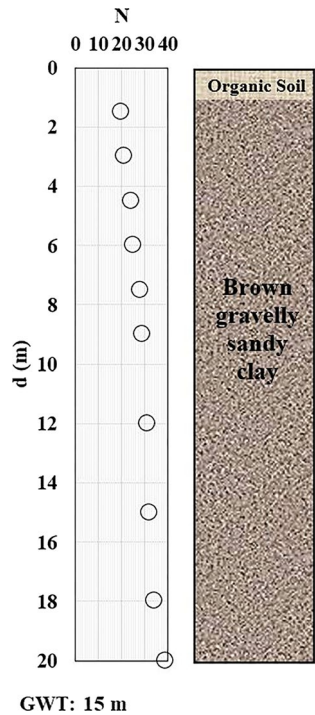
Fig. 35 Settlement observed (38°40′07.0″N 39°11′04.8″E/01.02.2020/15:47)

Fig. 36 Typical borelog for Elazig-Mustafa Pasa District (M. Gor, personal communication 2020)

pre-earthquake as well as additional seismically-induced fresher settlements were identi-fied and documented separately.

5.4 Mustafa Pasa District/Elazig

Mustafa Pasa District consists of Plio-Quaternary aged young sediments. Typical soil profiles are composed of brown gravelly sandy clay. Groundwater table is typically observed at 15-m depth. A representative lithology is presented in Fig. 36. V_{S30} for the region was measured as 300–350 m/s by MASW. Note that the borelog given in Fig. 36 reflects idealized soil conditions, which may not be representative for the whole district. A few structurally damaged residential buildings were documented in Mustafa Pasa District of Elazig Downtown. These had suffered from intensive cracking to partial collapse.

6 Performance of other structures

Field investigation work by the reconnaissance team was finalized with the inspection of various other structures including railway tracks, railway tunnels and water canals. Three structure were selected as representative examples of the performance of these other structures and summarized in Table 9. Figures 37, 38, 39 and 40 present the discussed sites' views.

7 Summary and conclusions

The M = 6.8 Elazig–Sivrice earthquake had occurred on the EAFZ, which was quite in terms of large magnitude events for the last century, on January 24, 2020 and resulted in 50, 155 and 8 collapsed buildings in the cities of Elazig, Malatya, and Diyarbakir, respectively. METU-Geotechnical reconnaissance team had arrived in the site within one week of the mainshock to collect and document perishable geotechnical engineering data in the form of permanent ground deformations, soil liquefaction or slope instability, etc. In addition, the seismic performance of earthfill and rockfill dams, tunnels and residential building foundation systems were documented, the recorded ground motions were analyzed and compared with the design-basis ground motions given in TSHM. Recorded ground motions for $R_{RUP} < 50$ km were lower than or equal to the design spectra with 72-year return period at short periods; while, the mid-long period (T > 0.5 s) ground motions were reached up to the design spectrum with 475-year return period at Puturge and Sivrice.

The reconnaissance route mostly concentrated on soil sites, which are composed of young alluvial deposits. These sites along Lake Hazar shores, Karakaya Dam Reservoir-Euphrates River shores, Malatya-Battalgazi and Elazig Downtown are predicted to be shaken by PGA_{1100} levels of 0.12–0.42 g, 0.05–0.11 g, 0.05 g, and 0.08 g respectively. The documented geotechnical field performances vary from widespread liquefaction-induced sand boils and lateral spreading to no signs of surface manifestations of permanent ground deformations or soil liquefaction. Samples were taken from the field to assess site soil conditions and liquefaction susceptibility. Sieve analyses performed on the sand ejecta confirmed their susceptibility to soil liquefaction. Available nearby borelogs from local site investigation database catalogs of Elazig and Malatya were compiled and assessed to perform preliminary liquefaction triggering analysis. Due to plastic cohesive soil layers dominating the alluvial geological setting of Elazig and Malatya Downtowns, the number of potentially liquefiable non-plastic saturated soil layers were assessed to be limited which were predicted not to have liquefied during the event, consistent with reconnaissance

Table 9 Summary of the performance of other structures

Site name (coordinates)	Median PGA (g) based on possible V_{S30}	Remark
Site 3 (38°26′49.5″N 39°18′33.4″E)	0.41–0.42	The railway tracks, were observed to have experienced no damage
Site 5 (38°26′43.7″N 39°20′40.8″E)	0.37–0.40	Guney Kurtalan Express Train services was uninterrupted after the earthquake, as documented in Fig. 34
Site 10 (38°28′52.8″N 39°27′18.2″E)	0.16–0.25	No damage was observed in a relatively short (~ 15 m long) railway tunnel, which was constructed at the toe of a highly weathered rock steep slope at slope. Tunnel has been possibly designed to eliminate toe excavations, which may trigger slope instability problems
Site 23 (38°26′00.4″N 38°21′44.1″E)	–	A water canal located near Battalgazi was documented with no signs of damage. Note that the observed cracks were dated older and are not associated with the recent earthquake event

Fig. 37 A view of railway tracks without any damage at Sivrice (38°26′49.5″N 39°18′33.4″E/31.01.2020/13:29)

Fig. 38 A view of the tunnel and Guney Kurtalan Express Train passing by (38°26′43.7″N 39°20′40.8″E/31.01.2020/13:54 & 38°26′56.9″N 39°21′16.7″E/31.01.2020/13:59)

findings. Lake Hazar liquefaction cases were assessed on the basis of simplified procedures and Cetin et al. (2018) liquefaction triggering predictive model. Consistent with field observations, these case history sites were concluded to be liquefied during the event.

Fig. 39 A railway tunnel and rails exhibiting no damage (38°28′52.8″N 39°27′18.2″E/31.01.2020/15:08 & 38°28′53.2″N 39°27′18.4″E/31.01.2020/15:09)

Fig. 40 Water canal in Dolamantepe Neighborhood of Battalgazi Village (38°26′00.4″N 38°21′44.1″E/01.02.2020/9:25)

A number of rock falls was mapped, based on back analyses of which probable peak ground velocities at the rockfall sites were speculated to vary in the range of 4–6 m/s. Consistently, the peak ground velocity (PGV) at this site was estimated to fall in the range of 5–19 m/s by ASK14.

There exist six hydraulic dams in Euphrates basin, namely Karakaya, Dedeyolu, Cip, Kapikaya Turgut Ozal, Keban and Boztepe Recai Kutan Dam, which are predicted to be shaken by peak ground acceleration ($PGA_{VS30=1100\ m/s}$) values to vary in the range of 0.03–0.23 g. The dams were inspected after the event by a group of engineers from the DSI and METU reconnaissance teams. No signs of seismically induced permanent deformations were observed, except 3–8 mm wide, longitudinal surface cracks observed along the crest of Dedeyolu Dam. The permanent deformations by Makdisi and Seed (1977) procedure were estimated to vary in the range of 1–5 mm, which were concluded to be in good agreement with the observed width of cracks in the crest. Additionally, despite lack of surface manifestations, a maximum of 2 cm settlement was recorded by magnetic extensometers installed in the clay core of Keban Dam. To test their functionality, Karakaya and Keban Dams' spillway gates were opened and closed, after which their elastic responses during and after the event were confirmed.

Damages on a number of non-engineered masonry, and reinforced concrete structures was also observed. Some of these structures suffered from intensive cracking, partial collapse, whereas some others experienced no evident damage. Readers are referred to Cetin et al. (2020) and METU EERC (2020) for in depth discussion of these structural damages. The documented foundation performances vary from no signs of permanent ground deformations to 1–3 cm settlement and 1–2 cm lateral movements.

As the concluding remark, these reconnaissance findings are presented with the intention of future more in-depth follow-ups, the findings of which are hoped to produce valuable case histories with potential use in the development of new predictive models or in the calibration of existing ones.

References

Abrahamson NA, Silva WJ, Kamai R (2014) Summary of the ASK14 ground motion relation for active crustal regions. Earthq Spectra 30(3):1025–1055

Akkar S, Aldemir A, Askan A, Bakir S, Canbay E, Demirel IO, Erberik MA, Gulerce Z, Gulkan P, Kalkan E, Prakash S, Sandikkaya MA, Sevilgen V, Ugurhan B, Yenier E (2011) 8 March 2010 Elazig-Kovancilar (Turkey) Earthquake: Observations on ground motions and building damage. Seismol Res Lett 82(1):42–58

Akkar S, Azak T, Can T, Ceken U, Demircioglu Tumsa MB, Duman TY, Erdik M, Ergintav S, Kadirioglu FT, Kalafat D, Kale O, Kartal RF, Kekovali K, Kilic T, Ozalp S, Altuncu Poyraz S, Sesetyan K, Tekin S, Yakut A, Yilmaz MT, Yucemen MS, Zulfikar O (2018) Evolution of seismic hazard maps in Turkey. Bull Earthq Eng 16(8):3197–3228

ASTM International (2011) D2435/D2435M—11 Standard one-dimensional consolidation properties of soils using incremental loading. West Conshohocken, PA

ASTM International (2016) D7928-17 Standard test method for particle-size distribution (gradation) of fine-grained soil using the sedimentation (hydrometer) analysis. West Conshohocken, PA

ASTM International (2017a) D2487-17e1 Standard Practice for Classification of Soils for Engineering Purposes (Unified Soil Classification System), West Conshohocken, PA

ASTM International (2017b) D6913/D6319M-17 Standard Test Method for Particle-Size Distribution (Gradation) of Soils Using Sieve Analysis. West Conshohocken, PA

Boore DM, Atkinson GM (2008) Ground-motion prediction equations for the average horizontal component of PGA, PGV, and 5%-damped PSA at spectral periods between 0.01 s and 10.0 s. Earthq Spectra 24(1):99–138

Boore DM, Stewart JP, Seyhan E, Atkinson GM (2014) NGA-West 2 equations for predicting PGA, PGV, and 5%-damped PSA for shallow crustal earthquakes. Earthq Spectra 30:1057–1085

Boulanger RW, Idriss IM (2012) Probabilistic standard penetration test–based liquefaction–triggering procedure. J Geotech Geoenviron Eng 138(10):1185–1195. https://doi.org/10.1061/(ASCE)GT.1943-5606.0000700

Brandenberg SJ, Zimmaro P, Stewart JP, Kwak DY, Franke KW, Moss RE, Cetin KO, Can G, Ilgac M, Stamatakos J, Weaver T (2020) Next-generation liquefaction database. Earthq Spectra 36(2):939–959. https://doi.org/10.1177/8755293020902477

Cetin K, Seed R, Kayen R, Moss R, Bilge H, Ilgac M, Chowdhury K (2018) The use of the SPT-based seismic soil liquefaction triggering evaluation methodology in engineering hazard assessments. Methodsx 5:1556–1575. https://doi.org/10.1016/j.mex.2018.11.016

Cetin KO, Ilgac M, Can G, Cakir E, Soylemez B (2020) 24 January 2020, Sivrice–Elazig–Turkey Earthquake Reconnaissance Report. DesignSafe-CI. https://doi.org/10.17603/ds2-9jz1-e287.

Cheloni D, Akinci A (2020) Source modelling and strong ground motion simulations for the 24 January 2020, Mw 6.8 Elazig Earthquake, Turkey. Geophys J Int 223(2):1054–1068. https://doi.org/10.1093/gji/ggaa350

Chiou BSJ, Youngs RR (2008) Chiou-Youngs NGA ground motion relations for the geometric mean horizontal component of peak and spectral ground motion parameters. Earthq Spectra 24:173–215

Chiou BSJ, Youngs RR (2014) Update of the Chiou and Youngs NGA model for the average horizontal component of peak ground motion and response spectra. Earthq Spectra 30:1117–1153

Dakoulas P, Gazetas G (1985) A class of inhomogeneous shear models for seismic response of dams and embankments. Soil Dyn Earthq Eng 4(4):166–182

Duman TY, Emre O (2013) The East Anatolian Fault: Geometry, segmentation and jog characteristics. Geological Society London, Special Publications

Gulerce Z, Kargoiglu B, Abrahamson NA (2016) Turkey-adjusted NGA-W1 horizontal ground motion prediction models. Earthq Spectra 32(1):75–100

Gulerce Z, Tanvir Shah S, Menekse A, Ozacar AA, Kaymakci N, Cetin KO (2017) Probabilistic seismic-hazard assessment for East Anatolian fault zone using planar fault source models. Bull Seismol Soc Am 107(5):2353–2366. https://doi.org/10.1785/0120170009

Kale O (2019) Some discussions on data-driven testing of ground-motion prediction equations under the Turkish ground-motion database. J Earthquake Eng 23(1):160–181

Kale O, Akkar S, Ansari A, Hamzehloo H (2015) A ground-motion predictive model for Iran and Turkey for horizontal PGA, PGV, and 5% damped response spectrum: investigation of possible regional effects. Bull Seismol Soc Am 105(2A):963–980. https://doi.org/10.1785/0120140134

Kavruk F (2003) Seismic behavior of embankment dams. Middle East Technical University MSc dissertation

Kurtulus C, Sertcelik F, Sertcelik I, Kuru T, Tekin K, Ateş E, Apak A, Kokbudak D, Sezer S, Yalcin D (2019) Determination of the national strong ground motion recording stations' soil parameters. National Earthquake Research Program (UDAP), AFAD **(in Turkish)**

Makdisi FI, Seed HB (1977) A simplified procedure for estimating dam and embankment earthquake-induced deformations in dams and embankments. Earthqukae Engineering Research Center Report No: UCB/EERC-77/19

METU EERC (2020) The Elazig-Sivrice Earthquake (24 January 2020 M_w=6.8) field observations on seismic and structural damage. Middle East Technical University Earhquake Engineering Research Center Report No: METU/EERC 2020–01

MTA (General Directorate of Mineral Research and Exploration) (2020) 24 Ocak 2020 Sivrice (Elazig) Depremi (M_w=6.8) saha gözlemleri ve değerlendirme raporu, Ankara. https://www.mta.gov.tr/images/duyuru_ek/belgeler/609_07-02-2020_2b82a14b.pdf **(in Turkish)**

Pousse-Beltran L, Nissen E, Bergman EA, Cambaz MD, Gaudreau É, Karasozen E, Tan F (2020) The 2020 M_w 6.8 Elazig (Turkey) Earthquake reveals rupture behavior of the East Anatolian Fault. Geophys Res Lett. https://doi.org/10.1029/2020GL088136

RocFall 2019 v7.0. (2019) Software for risk analysis of falling rocks on steep slopes. RocScience Inc., Toronto

Sandikkaya MA, Yilmaz MT, Bakir BS, Yilmaz O (2010) Site classification of Turkish national strong-motion stations. J Seismolog 14(3):543–556

Saroglu F, Emre O, Kuscu I (1992) The east anatolian fault zone of Turkey. Ann. Tectonicae VI:99–125

Saygili G, Rathje EM (2008) Empirical predictive models for earthquake-induced sliding displacements of slopes. J Geotech Geoenviron Eng 134(6):790–803. https://doi.org/10.1061/(ASCE)1090-0241(2008)134:6(790)

Seed HB, Idriss IM (1971) Simplified procedure for evaluating soil liquefaction. J Soil Mech Found Div 97(9):1249–1273. https://doi.org/10.1061/JSFEAQ.0001662

Seed HB, Tokimatsu K, Harder LF, Chung RM (1985) Influence of SPT procedures in soil liquefaction resistance evaluations. J Geotech Eng 111(12):1425–1445. https://doi.org/10.1061/(ASCE)0733-9410(1985)111:12(1425)

TBDY (2019) Turkish building earthquake code. Ministry of Interior, Ankara (**in Turkish**)

Tsuchida H (1970) Prediction and countermeasure against the liquefaction in sand deposits. Abstract of the Seminar in the Port and Harbor Research Institute **(in Japanese)**